Remote Sensing: Classifying Urban Land Use Types with Satellite Imagery

A Thesis submitted to the faculty of
San Francisco State University
In partial fulfillment of
the requirements for
the Degree

Master of Science

In

Geographic Information Science

by

Philip James Lynch

San Francisco, California

May 2020

CERTIFICATION OF APPROVAL

I certify that I have read Remote Sensing: Classifying Urban Land Use Types with Satellite Imagery by Philip James Lynch, and that in my opinion this work meets the criteria for approving a thesis submitted in partial fulfillment of the requirement for the degree Master of Science in Geographic Information Science at San Francisco State University.

L. Blesius

Leonhard Blesius, Ph.D.
Associate Professor

Ellen Hines, PhD

Ellen Hines, Ph.D.
Professor

Remote Sensing: Classifying Urban Land Use Types with Satellite Imagery

Philip James Lynch
San Francisco, California
2020

An accelerating trend of global urbanization and subsequent environmental impacts makes frequently updated land use and land cover (LULC) maps critical. LULC maps have been widely created through classification of remotely sensed imagery. Maps of urban areas have been both dichotomous (urban or non-urban) and entailing of discrete urban types. This study incorporated multispectral built-up indices designed to enhance satellite imagery to develop new urban classification schemes. The indices examined are the New Built-up Index (NBI), the Built-up Area Extraction Index (BAEI), and the Normalized Difference Concrete Condition Index (NDCCI). Landsat Level-2 data covering the city of Miami, FL, USA was leveraged with geographic data from the Florida Geospatial Data Library and Florida Department of Environmental Protection to develop and validate new methods of supervised and unsupervised classification of urban area. NBI was found to be useful for classifying urban features through object-oriented image analysis. BAEI was utilized to visualize and track urban development as a low-high gradient. NDCCI was composited with NBI and BAEI as the basis for a robust urban intensity classification scheme superior to that of the urban intensities featured in the 2016 USGS National Land Cover Database. BAEI, implemented as a shadow index, was incorporated in a novel infill geosimulation of high-rise construction. The findings suggest that the proposed classification schemes are advantageous to the process of creating more detailed LULC maps in response to the rising global demand for them.

I certify that the Abstract is a correct representation of the content of this thesis.

L. Blesius — 24.5.2020

Chair, Thesis Committee — Date

PREFACE AND/OR ACKNOWLEDGEMENTS

Thank you to the faculty and staff of San Francisco State University's Department of Geography and Environment for providing the chance to grow as a student in the field of remote sensing. Nancy Wilkinson for hosting an excellent graduate program, Jerry Davis for enormous support in understanding geographic and environmental concepts, as well as Anna Studwell and Quentin Clark for continuous lab support and access to facilities. Special thanks to my advisors, Leonhard Blesius for providing his insight and always remaining approachable to educate in the matter of remote sensing and Ellen Hines for her insight and teaching me the rigors of scientific writing. The study detailed in this manuscript is dedicated to the discipline of geomatics, and gracious acknowledgment is given to each author of incorporated scientific papers covering the subjects of urban remote sensing, image classification, and geosimulations. I intend to clarify the research frontier of discriminating the properties of urban surfaces by utilizing satellite imagery in conjunction with geographic information systems by introducing new methodology.

TABLE OF CONTENTS

TABLE OF CONTENTS

LIST OF TABLES

LIST OF FIGURES

Figure Page

1. Introduction

Today, the world's rapidly developing trend of urbanization has made frequently updated surface maps critical (Guan et al., 2011; Rahimi, 2016; Seto et al., 2012; Sun et al., 2007). Land use and land cover (LULC) maps are advantageous for purposes of government planning, environmental management, disaster management, and education of the general public on the status of global development. The impacts of urbanization for the environment include triggering potentially harmful feedback such as climate change, reducing water quality, and replacement of nature by human construction (Mohan & Kandya, 2015; Nelson et al., 2009; Zia et al., 2015). The link between urbanization and environmental impacts can be analyzed by mapping their extent and severity in relation to urban expansion (Han & Xu, 2013; Pei et al., 2018; Tang et al., 2015). LULC maps may serve as tools of emergency response to disasters such as fires, earthquakes, and floods where the extent and severity of the disasters can be displayed and analyzed to support response measures. The problem of producing the detailed urban LULC maps on a large scale can be solved with satellite remote sensing.

Satellite remote sensors typically feature multiple spectral bands for use in analysis, where each band may be advantageous given the properties of materials identifiable in different parts of the light spectrum (Bouzekri et al., 2015; Jieli et al., 2010; Samsudin et al., 2016; Zha et al., 2003). Satellite remote sensors take a bird's-eye view of LULC changes related to urban growth. While high-resolution (~1m^2) remote sensing has proven to be very useful for mapping the extent of urbanization as well as for

mapping the presence of individual building footprints, the research presented here focuses primarily on satellites of moderate resolution (10-30m^2) (Bouzekri et al., 2015). Moderate-resolution data may be sufficient for mapping urban extent and is typically available for free in large time-series volumes compared to high-resolution data, which is expensive to acquire and making it unsuitable for institutions with limited budgets.

Typically, satellite image analysts take a dichotomous approach to LULC mapping, classifying image cells as either urban or non-urban (As-syakur et al., 2012; Benkouider et al., 2019; Bouzekri et al., 2015; He et al., 2010; Jieli et al., 2010; Rasul et al., 2018; Waqar et al., 2012; Xu, 2008; Zha et al., 2003). LULC maps often depict the encroachment of urban sprawl expanding into the natural landscape. Still, some cities do not grow outwardly because of physical constraints (other cities, terrain, water bodies, etc.) or should not grow outwardly because of planning regulations. The world population is expected to increase from ~8 billion currently to 10 billion in three decades, driving the impact of problems associated with urbanization to new levels (Seto et al. 2012; UN DESA, 2017). In response, governments are enacting smart growth policies meant to limit outwardly expanding cityscapes into compact, walkable urban areas with higher populations (Rahimi, 2016). Smart growth implies that environmental impacts are lessened by condensing urban infrastructure (Rahimi, 2016). Therefore, the drawing of infill development policies is a foremost solution to the problems associated with the outward expansion of cityscapes against the natural landscape (Rahimi, 2016). The term infill development refers to the rededication of urban land to new construction. Simply,

urban growth within the confines of the cityscape, such as the development of vacant lots, redevelopment of run-down neighborhoods, and conversion of parks to construction.

An inventory of urban land can be obtained through field methods as well as the classification of aerial photographs and satellite imagery and cataloged as data in a geographic information system (GIS). Classifying every land use plot specifically as possible may take a long time, where the necessary geographic view can be achieved more efficiently through a large-scale remote sensing classification. Numerous attempts to classify urban land use by discrete types are on record in scientific journals. Among the methods that may be implemented to create such maps include supervised classification requiring class training sets such as parametric Gaussian maximum likelihood (GML) or non-parametric Support Vector Machine (SVM), iterative unsupervised classification such as k-means and ISODATA, and object-oriented image analysis (OBIA) segmentation (Abbas et al., 2016; Cabral, 2007; Ettehadi et al., 2019; Igun, 2017) While classifiers by themselves are used to create maps featuring multiple urban types, the process can be refined and simplified using multispectral unsupervised classification formulas called spectral enhancements.

Remote sensing spectral enhancements are formulas used to transform multispectral data retrieved from a sensor into indexed quantities useful for analyzing a target environment, isolating target features, and indexing those features into identifiable classes (Beck et al., 1990; Bouzekri et al., 2015; Jieli et al., 2010; Samsudin et al., 2016; Zha et al., 2003). For instance, measurements of solar radiation reflecting from Earth's

surface to a satellite sensor can be manipulated to yield a description of plant biology, the presence of bare soil, or a state of urbanization (Bouzekri et al. 2015). For example, Zha et al. (2003) introduced a method for extracting urban features from satellite data using a spectral enhancement. The Normalized Difference Built-up Index (NDBI) was used to extract urban features of Nanjing, China from Landsat 5 Thematic Mapper (TM) $30m^2$ satellite data. It enhances the spectral response differences that exist between shortwave infrared (SWIR) and near-infrared (NIR) bands to separate urban from non-urban areas in an image. The authors reported an accuracy of 92.6% based on an assessment of 68 randomly distributed points in their study area and assert NDBI increases the classification accuracy of urban features compared to the GML classifier. Ettehadi et al. (2019) mapped the land cover of Istanbul by classifying enhanced images, derived from Sentinel-2A 10-$20m^2$ data, using SVM. The Normalized Difference Tillage Index was used to highlight urban features as part of a three-band composite image, including the Red-edge-based Normalized Difference Vegetation Index, and the Modified Normalized Difference Water Index. They delineate asphalt, industrial land use, and other built-up as part of their classification scheme. The reported producer and user accuracies are 85.71% and 100% for asphalt areas, 98.28% and 81.43% for industrial areas, and 93.28% and 92.25% for other built-up. It is of critical notice that differences in environmental factors like lighting, the complexity of land cover, etc. that occur between regions will impact the performance of spectral enhancements (Bouzekri et al. 2015).

In addition to static classification maps, urban growth models, called geosimulations, are used to generate land cover maps of predictable conditions by assigning transition probabilities and potentials to maps derived from remote sensing (Guan et al., 2011; Rahimi, 2016; Sun et al., 2007). An artificial neural network (ANN) is a dynamic computerized model that attempts to duplicate human actions and learning functions. Multilayer Perceptron (MLP) is the most commonly implemented ANN. A backpropagation algorithm, learning based on gradient descent when the network informs itself of a prediction error, is useful for predicting complex values (Marius et al., 2009). The challenges of operating MLP ANN include configuring its parameters and establishing the correct inputs used to calculate a prediction (Marius et al., 2009).

According to Guan et al. (2011), the Markov Chain is an empirical method of land change modeling implemented to generate a transition probability matrix that serves as a basis for space-time-series analysis. A first-order Markov Chain model is defined as a chain, where the probability of the future state depends only on the present state and not on preceding states, and every point in time is the next step. It is appropriate to incorporate this technology in modeling urban systems because the transformation properties of land change have to do with predictable transitions and steady states (Guan et al., 2011).

Rahimi (2016) utilized a combination of GIS, satellite remote sensing, and an MLP ANN in an attempt to map potential infill development for the city of Tabriz, Iran. Urban land cover was classified, cell-by-cell, as either urban or subject to infill

development. LULC classifications were derived from Landsat 5 data for 1989 and Satellite Pour l'Observation de la Terre (SPOT) $10m^2$ data for 2005. The classifications were cross-referenced with geographic predictor variables such as distance from roads and population density using an MLP ANN geosimulation, thus predicting urban land cover for 2021. Additionally, Sun et al. (2007) modeled the growth of Calgary, Canada, using a Cellular Automata/Markov Chain combination model. They predicted change, using classified Landsat 5 data from 1985 and 1992, regarding the presence of residential and commercial, industrial, transportation, and park development compared to vacant areas and water bodies. Suitability maps of Calgary's "Future Conceptual Urban Structure" were created for each class, merged, and used as a predictor. The researchers were able to achieve favorable results according to a cellular accuracy assessment using data of known conditions of the predicted year, 1999.

The purpose of this paper is to advance our current understanding of the processes of leveraging remote sensing to identify discrete urban land use types for incorporation into modeling schemes such as static mapping and geosimulations. The research focused on feature extraction and classification with the implementation of spectral enhancements. The analysis evaluated the unique spectral properties of select remote sensing enhancements designed to enhance construction features from the natural landscape for the creation of new classification schemes that delineate urban land use types. The enhancements analyzed are the New Built-up Index (NBI) by Jieli et al. (2010), the Built-up Area Extraction Index (BAEI) by Bouzekri et al. (2015), and the

Normalized Difference Concrete Condition Index (NDCCI) by Samsudin et al. (2016). Urban intensities published by the USGS in the 2016 National Land Cover Database (NLCD) are analyzed for classification errors, and a corrected classification was modeled with the NLCD 2016 Percent Developed Imperviousness product in tandem with the SVM supervised and Iso Cluster unsupervised classifiers. A novel geosimulation of high-rise development was performed with land use classifications derived from the BAEI as a shadow index. The aim is to propose new schemes based on enhancements for classifying urban land using:

1. Classification by object
2. Classification by gradient
3. Classification by intensity
4. Classification by focalized transition potential

The research was conducted on a place with satellite coverage, where urban growth modeling is highly relevant to environmental sustainability and can be validated using a sufficient volume of ground-truth data.

2. Method

2.1. Study Area

Miami, FL, USA is located on the southeastern tip of Florida at 25° 46' 29.8128" N / 80° 11' 9.5604" W, spans ~143km^2, and serves as the Miami-Dade County seat (see **Figure 1**). The land use types comprising the city are primarily residential, commercial, and industrial. Miami poses a unique challenge to the science of urban remote sensing. It does not grow outwardly because other cities and development border its western periphery, and its eastern boundary is the coast. It is a rapidly developing metropolis with a recorded population increase of ~350,000 in 1980 to ~486,000 in 2020 (World Population Review, 2020). Miami-Dade County has enacted development concurrency policies meant to force a compact urban design by slowing sprawl and promoting infill development (Kim et al., 2014). For instance, some areas of Miami became hotspots for construction of multifamily housing between 1995-2004, after the inception of Transportation Concurrency Exception Areas that allow for infill development despite traffic and accessibility limits (Kim et al., 2014). A coastal setting containing sensitive marine environments makes this city a highly relevant target for an inquisition into environmental conservancy by actively managing urban growth. If remote sensing is implemented as a means of monitoring Miami's growth, it should be modeled to account for upward growth. A collection of cloud-free Landsat data is available from the USGS in

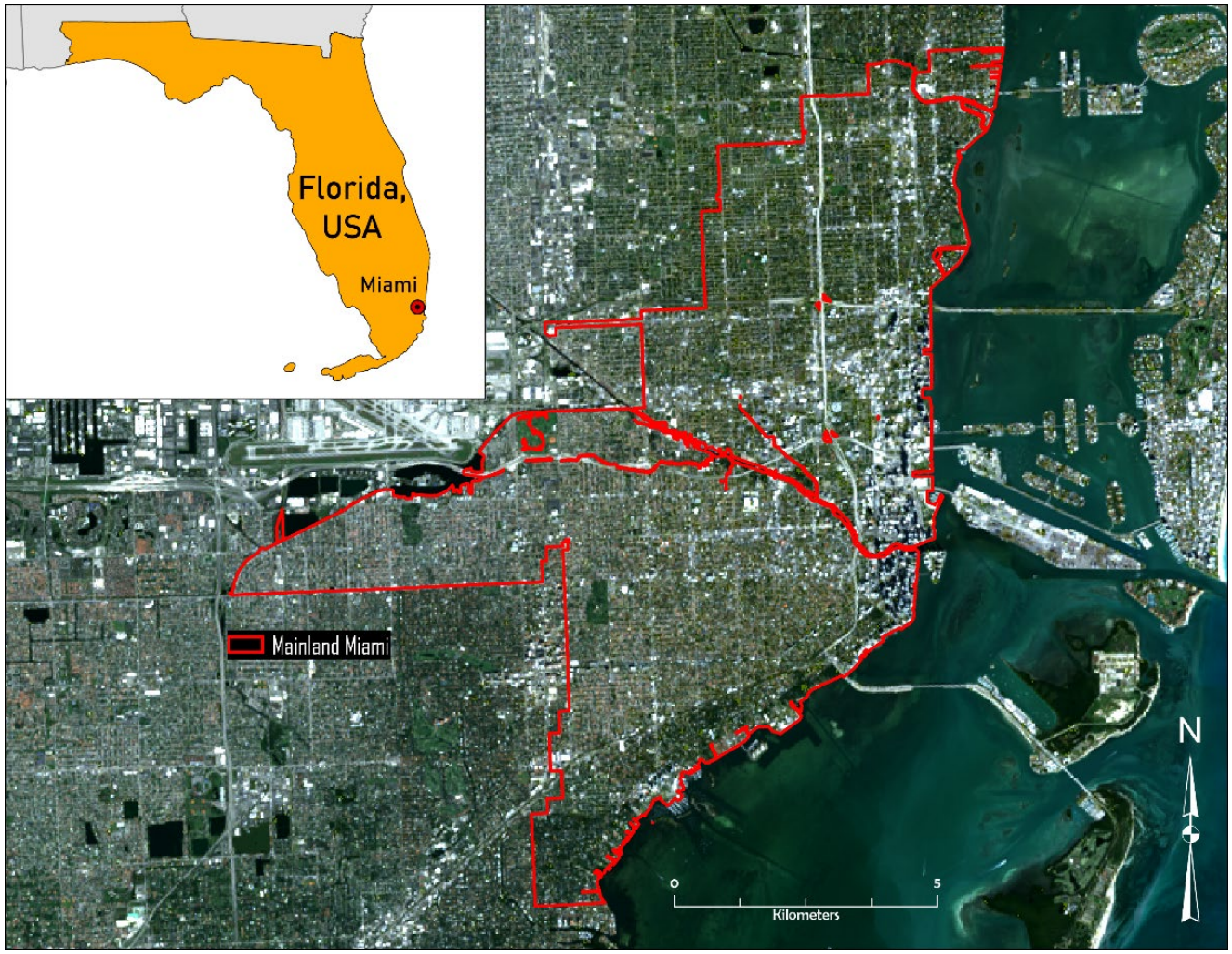

Figure 1. Miami sits on the southeastern tip of Florida. The city is enclosed by the Biscayne Bay and Atlantic Ocean to the east, and urbanized parts of Miami-Dade County inland.

addition to volumes of GIS data provided by the state of Florida and Miami-Dade County.

2.2. Data Sources

Vector GIS data of the study area were retrieved from Miami-Dade County Open GIS. That data includes shapes of the Miami municipal boundary in addition to county water features and the shoreline. Florida neighborhood shapes were retrieved from Zillow Real Estate Listings. Finally, shapes of Florida LULC designations were retrieved from the Florida Geographic Data Library (FGDL) and the Florida Department of Environmental Protection (FDEP) Geospatial Open Data. The GIS data are used to clip and analyze select portions of satellite data from the National Aeronautics and Space Administration (NASA) Landsat satellite series. NLCD 2016 data were published by the United States Geological Survey (USGS).

According to the USGS (n.d.), the $30m^2$ Landsat Surface Reflectance Level-2 science data that is available free to the public from their EarthExplorer website is designed to support the analyses of land change science. Level-2 data is preprocessed with both georeferencing as well as atmospheric corrections to normalize every image in the dataset for comparison. Level-2 Landsat 5 TM and 7 Enhanced Thematic Mapper + (ETM+) data receive atmospheric corrections in the form of 6S (Second Simulation of a Satellite Signal in the Solar Spectrum) meant to minimize the influence of water vapor, ozone, geopotential height, aerosol, and elevation on spectral returns. Similarly, Landsat

8 Operational Land Imager (OLI) data is corrected with an internal satellite algorithm. All Level-2 images used for this study are georeferenced to the Universal Transverse Mercator (UTM) Zone 17N projected coordinate system. Subsequently, all other data was initially projected to this system to facilitate analysis, except for the NLCD products (USGS, n.d).

The imagery used in this study includes Landsat 5 data for the dates of 11/02/1985, 11/06/1998, 10/24/1999, 11/20/2003, 11/17/2008, 10/19/2009, 11/02/2011, Landsat 7 data for the date of 02/05/2000, and Landsat 8 data for the dates of 10/17/2014 and 10/22/2016. The temporal sequencing of the data was intended to minimize the spectral influence of differences that will occur because of seasonal conditions. Due to sensor saturation, the data may contain minor errors that pitch some cell values outside of the 0-1 range of proper reflectance values. These cells are screened out of each band during geoprocessing to preserve analytical accuracy.

2.3. Workflow

The workflow displayed in **Figure 2** emphasizes seamless automation. ESRI's ArcGIS (ESRI, 2020) was the software used in most of the analysis; for geoprocessing, geospatial analysis, and cartography. IDRISI TerrSet (Clark Labs, 2015) was used for geosimulating future land use using the Land Change Modeler (LCM) module for MLP ANN Markov Chain analysis.

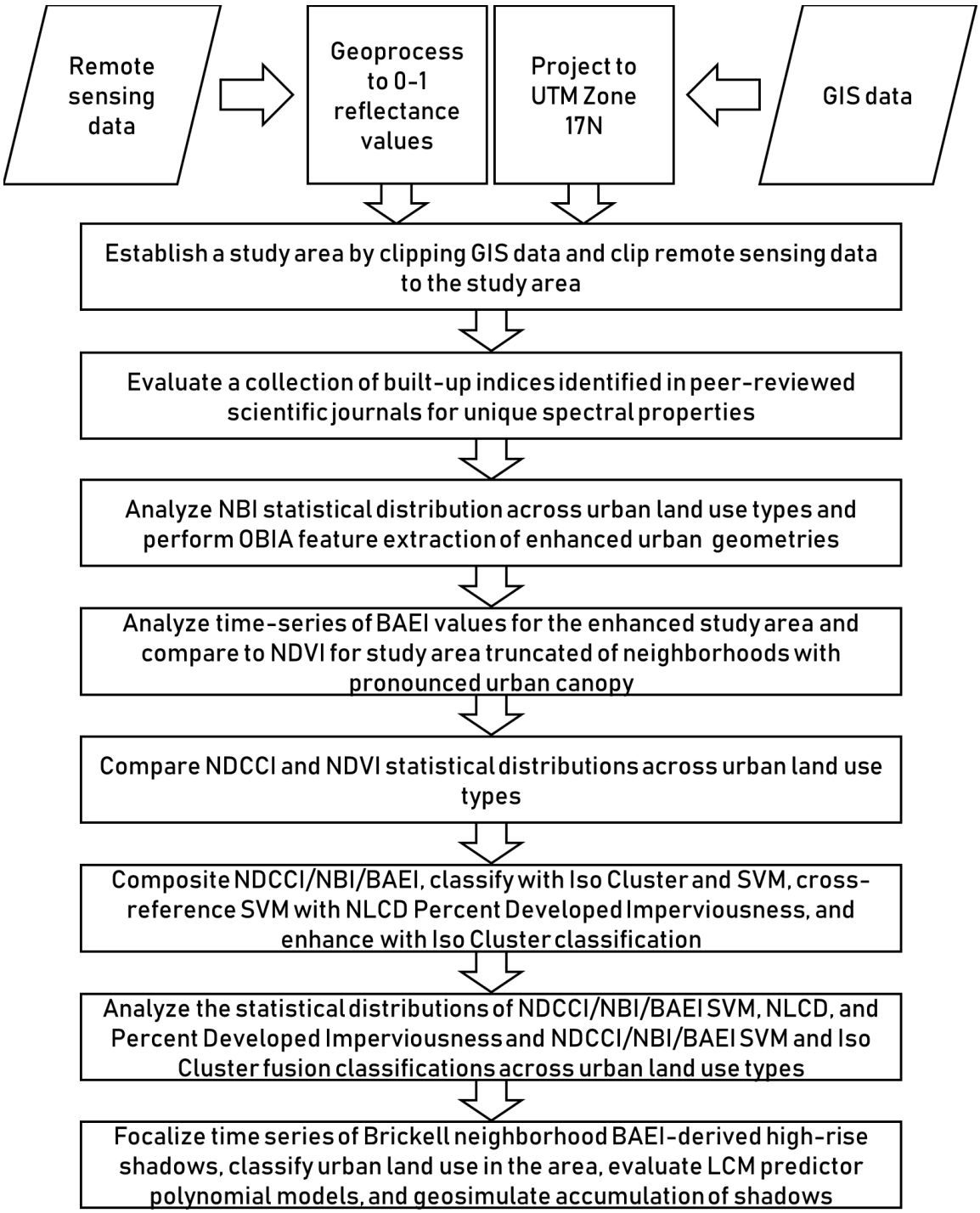

Figure 2. General workflow diagram.

2.4. Evaluation of Published Built-up Indices

Landsat data were used to evaluate eleven remote sensing spectral enhancements; nine designed to extract urban features from moderate resolution data; one designed to extract urban features from SPOT data, and one designed to assess the quality of building materials with high-resolution data. A list of these enhancements is given in **Table 1**.

The three enhancements selected for further analysis were NBI, BAEI, and NDCCI (see **Figure 3**). Upon visual assessment, NBI showed pronounced differences between areas of Miami that are known to possess business infrastructure compared to those that are known to possess no infrastructure or residential land use. Therefore, it was selected for further evaluation regarding its usefulness for serving as the basis of an object-oriented urban land use classification scheme.

Jieli et al. (2010) developed NBI with Landsat 5 data to automate the process of mapping residential areas of Changzhou City, China. The researchers report an overall accuracy of 90% based on a survey of 50 random points in their study area. An NBI raster calculated from the 2016 Landsat 8 data was clipped to the shape of Miami without feature extraction thresholding. While visual assessment yielded the conclusion that it is easy to spot differences between one type of urban feature and another in the enhanced image, the point requires further elaboration. Noticeable differences exist among land cover types captured in satellite data between the red, NIR, and SWIR1 bands, and the NBI band arrangement yields an unsupervised classification where the brightest features

Table 1. Built-up indices found in scientific journals evaluated for unique spectral properties.

Name of Index	Author(s)	Formula	Accuracy	Study Area
The Enhanced Built-up and Bareness Index (EBBI)	As-syakur et al. (2012)	(SWIR1-NIR)/10*SQRT (SWIR1+THERMAL)	88.98%	Densapar, Indonesia
The Built-up Area Extraction Index (BAEI)	Bouzekri et al. (2015)	(RED+.3)/(GREEN+SWIR1)	92.66%	Djelfa, Algeria
The Built-up Index (BUI)	He et al. (2010)	(SWIR1-NIR)/(SWIR1+NIR)- (NIR-RED)/(NIR+RED)	86.3%	National Olympic Park, Beijing, China
The New Built-up Index (NBI)	Jieli et al. (2010)	(RED-SWIR1)/(NIR)	90%	Changzhou City, China
The Dry Built-up Index (DBI)	Rasul et al. (2018)	(BLUE-THERMAL)/(BLUE+THERMAL)- (NIR-RED)/(NIR+RED)	93%	Erbil, Iraq
The Normalized Built-up Area Index (NBAI) &	Waqar et al. (2012)	[(SWIR2-SWIR1)/GREEN]/ [(SWIR2+SWIR1)/GREEN]	86.87%	Islamabad, Pakistan
The Band Ratio for Built-up Area (BRBA)		(RED)/(SWIR1)	85.09%	
The Index-based Built-up Index (IBI)	Xu (2008)	2*SWIR1/(SWIR1+NIR)-[NIR/(NIR-RED)+ GREEN/(GREEN+SWIR1)]/ 2*SWIR1/(SWIR1+NIR)+ [NIR/(NIR-RED)+GREEN/ (GREEN+SWIR1)]	96.77%	Fuzhou City, South China
The Normalized Difference Built-up Index (NDBI)	Zha et al. (2003)	(SWIR1-NIR)/(SWIR1+NIR)	92.6%	Nanjing City, East China
Index Designed for Extracting Urban Features from SPOT Data				
The Modified Built-up Area Index (MBAI)	Benkouider et al. (2019)	[NIR+(1.57*GREEN)+(2.4*SWIR1)]/(1+NIR)	95% & 91%	Laghouat and M'Sila, Algeria
Index Designed for Determining Material Condition from High-resolution Data				
The Normalized Difference Concrete Condition Index (NDCCI)	Samsudin et al. (2016)	(NIR-GREEN)/(NIR+GREEN)	84.44%	University Putra Malaysia, Seri Kembangan, Malaysia

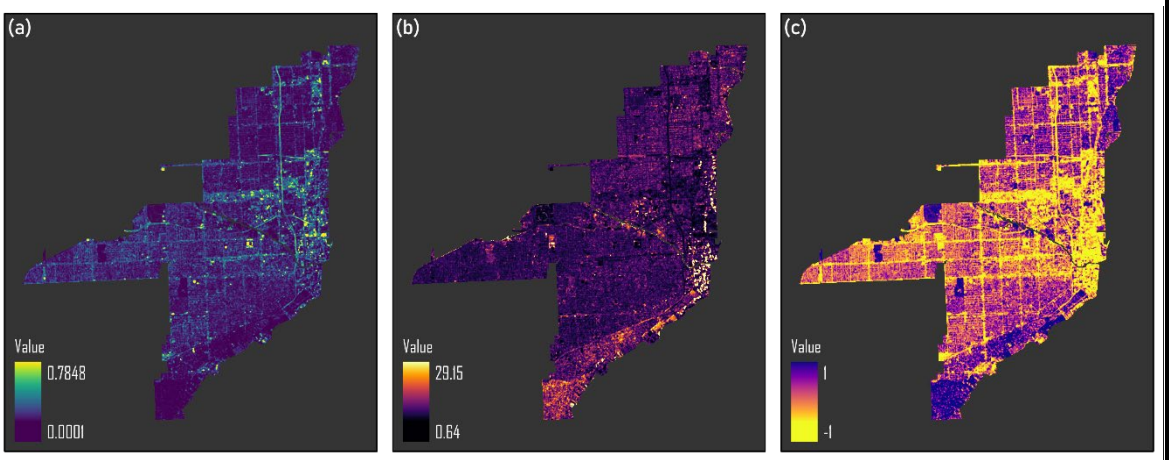

Figure 3. Select spectral enhancements derived from Landsat 8 OLI 10/22/16 data; (a) NBI, (b) BAEI, (c) NDCCI.

(typically urban or barren land) have the highest values (Jieli et al. 2010). Thus, NBI values for areas that are only urban will show enhanced brightness for features with high albedos, such as white concrete or the bare ground of construction sites. Subsequently, zonal statistics describing the central tendency of NBI values were calculated for each land use type featured in the FGDL data. It must be noted that FGDL data does not feature polygon geometries for streets and is advantageous because it contains additional details regarding the presence of industrial development compared to the data from FDEP. ArcGIS includes the Mean Segment Shift interactive OBIA tool for grouping parts of an image with similar properties into segments.

Phiri & Morgenroth (2017) define OBIA as the automatic digitization of homogenous image features. It works by grouping pixels into vectored segments and then assigning a class to like segments. Segments are defined by spectral, spatial, and geometric properties. Spectral detail refers to color characteristics, such as the difference

between one type of commercial construction and another. Spatial detail refers to identifiable differences in spatial characteristics, such as street lines compared to residential blocks. Geometric detail refers to the minimum size of an image segment, which can aggregate details on, for example, a pixel, block, neighborhood, or city level. The method is useful for avoiding a scattered, "salt and pepper" look typically associated with pixel-based classification methods (Phiri & Morgenroth, 2017).

The 2016 NBI was segmented into object primitives useful for identifying enhanced color intensity, object formation, and surface texture. An object encompassing industrial land use in the Little Haiti neighborhood of Miami was extracted by vectorizing a segment. The object was cross-referenced with the FGDL data to validate the usefulness of non-automatic, interactive segment selection as a classification method. While discrete urban types can be classified through OBIA feature extraction from NBI, there is still an additional need for analysis of the scale of development within classes. BAEI provides an enhanced view of the accumulation of construction material as a low-high gradient.

BAEI was selected for further evaluation regarding its usefulness for time-series change detection of a quantifiable increase in urban development (different grades of building presence) because of its range of non-linear values, which may prove useful for tracking shifts in urban morphology. In addition to a pronounced gradient, the BAEI feature extraction threshold separates high-rise shadows from the rest of the urban area.

BAEI is a high-precision, non-linear (the positive range of values extends beyond 0 to 1) feature extraction index developed with Landsat 8 data by Bouzekri et al. (2015) to automate the process of extracting built-up areas of Djelfa, Algeria. They report an accuracy of 92.66% based on a survey of 50 random points in their study area. Compared to the other built-up indices evaluated, it provides an expanded range of values that may be useful for classifying urban states with low-high values. An observable increase in the central tendency of BAEI values for an urban area, over a time-series, requires additional explanation.

Chrysoulakis (2003) utilizes NASA's Advanced Spaceborne Thermal Emission and Reflection Radiometer satellite, in combination with *in situ* data, to develop an estimation of the all-wave surface net radiation balance (NRB) for Athens, Greece. NRB is defined in the formula:

$$NRB = (1 - \alpha short)E + F\downarrow - F\uparrow$$

Here, αshort is surface total shortwave albedo; E is direct and diffuse shortwave irradiance on the surface; F ↓ is atmospheric downward longwave flux; F ↑ is total surface radiant exitance. Highly developed areas, such as business and stadiums, should possess a lower NRB because the higher albedos of bright construction material typify them and therefore absorb less radiation than areas with lower albedos, such as areas of medium development or vegetated spaces. Also, urbanization influences the distribution of heat fluxes related to NRB with a combination of drivers, including replacement of vegetation with construction, reduced surface moisture, and the complexity of urban

morphometry. BAEI is an expression of NRB, with low values for highly developed areas, mid-ranged values for medium development, and high values for areas that are vegetated or comprised of dark asphalt. Where BAEI values increase over time, the increase is linked to the influence of human beings on NRB, since NRB will rise for reasons linked to human development (Chrysoulakis, 2003).

To validate BAEI as automatic, unsupervised classification of different grades of building presence, an evaluation was made of the usefulness of BAEI to chronicle stages of urban growth for Miami using the mean as a measure of central tendency, including the influence of vegetation. BAEI was derived for six satellite images in a time-series spanning 1985-2016. If thresholds are not applied, BAEI rasters for Miami are highlighted by the formation of shadows cast by high-rise infrastructure in downtown neighborhoods. The visualizations need to be refined by omitting the formation of shadows to display the enhanced gradient visualization of an urban environment facilitated with BAEI.

The BAEI rasters were geoprocessed with conditional thresholds for Landsat 5/7 and Landsat 8. Note that conditional thresholds of 2.5 and 2.4 were assigned to Landsat 5/7 and Landsat 8 respectively to enhance BAEI visualizations. Those thresholds were determined through a process of raster histogram analysis. A different threshold for Landsat 8 is necessary because it possesses different spectral bandwidths and cannot be directly cross-referenced with the other two satellites. Cross-referencing can be

performed with post-classification image comparison and post-classification change detection.

A visual and statistical comparison was made of the BAEI time-series for the entire city. Due to the apparent influence of urban canopy in the southern portion of the city on BAEI values in the first time-series, a shape truncating the three southernmost neighborhoods was created. Rasters clipped to the truncated area were necessary to evaluate how well BAEI tracks the accumulation of constructed features over time as opposed to the accumulation of urban arbor. Further scrutiny was given to the truncated area concerning the influence of vegetation.

The Normalized Difference Vegetation Index (NDVI) has widely proven as useful in classifying the presence and vigor of plants visible in remote sensing data (Beck et al., 1990). NDVI values are linear, -1 + 1, with values in the direction of 1 indicating the presence of healthy vegetation.

$$NDVI = (NIR – RED) / (NIR + RED)$$

NDVI was calculated for the truncated area time-series for statistical and visual comparison. Note that Miami-Dade County does not possess significant arbor compared to other US urban areas, having 20% tree cover in 2016 (Hochmair et al. 2016). Additionally, zonal statistics for BAEI and NDVI were calculated using the truncated area for a time series of ten images spanning 1985-2016.

BAEI, utilized as a shadow index by not thresholding the raster, displays values for Miami with a pronounced division between the shadows cast by high-rises and other

urban area. Shadows are focalized and further analyzed by establishing a threshold to separate cells that highlight shadows. Subsequently, a time-series of urban land use classification maps incorporating the extracted shadow highlights was created to depict a formation trend. A geosimulation incorporating a 2003 and 2008 image time-series in combination with directional land use polynomial transition trends as predictors was performed to predict the construction of high-rise infrastructure for 2016 in the Brickell neighborhood. Consideration was given regarding how NBI and BAEI may be composited to take advantage of the useful properties of both enhancements.

It is possible to composite enhancements as an image stack, whereby the desirable properties of each enhancement can be translated to a single output. NDCCI derived from 2016 imagery visualized Miami's urban fabric as a network of streets containing pronounced areas of low-development, collections of homes, and varying stages of development in areas of business and dense transport. Consideration was given to NDCCI as the basis for an enhancement composite with NBI and BAEI based on a comparison of zonal statistics with NDVI referencing urban land use types. The composite was then classified to identify pronounced spectral groupings based on the feature extraction achieved by combining enhancements. That is, differing states of urban intensity are delineated according to their unique range within each built-up index.

NDCCI was developed by Samsudin et al. (2016) with data from the Worldview-3 satellite to assess the condition of concrete roofs in high-resolution data. Gu et al. (2018) considered the usefulness of the index for extracting building shapes from high-

resolution data. Where NDVI enhances the difference between near-infrared and red bands, NDCCI compares the difference between the green band. NDCCI may be implemented to assess the presence and quality of construction compared to the ability of NDVI to assess the presence and vigor of vegetation. Zonal statistics were calculated using the FDGL data to evaluate the way NDCCI groups discrete urban types compared to NDVI, both derived from 2016 imagery. Considering an observed homogenization of spectral responses within discrete urban types by NDCCI, the index is likely to be useful for identifying differences between urban land use types with a classifier when composited with NBI and BAEI.

NBI orders the brightness of urban features from low-high, BAEI gives an order to NRB, and NDCCI gives higher values according to the difference in spectral response between NIR and green wavelengths (high for vegetated areas and lower according to the extent of development). Moreover, it is important to visualize the differences between a classification performed with NDCCI to one performed with NDVI to gain a better understanding of why it is advantageous to incorporate an index designed to enhance construction compared to one designed to enhance vegetation. Therefore, composites were created for NDCCI/NBI/BAEI and NDVI/NBI/BAEI with 2016 imagery and analyzed with the Iso Cluster unsupervised classifier by Ball & Hall (1965). It must be noted that the classifications performed here and henceforward were done to make comparisons with and improve upon NLCD 2016 urban intensity data, and the enhancements were conditionally processed to only include cells classified as urban by

the USGS. That classification contains errors in the study area, where some vegetated areas are incorrectly classified as non-urban.

2.5. Classification of a Three-enhancement Composite

Both the NDCCI/NBI/BAEI and NDVI/NBI/BAEI composites were classified with Iso Cluster using the ArcGIS default settings. The classification output was visually assessed and reclassified to establish an interpretation of low-to-high urban development, in terms of arbitrary classes named Urban 1-5. Areas in classes 1-3 are typically open space, vegetated, or residential, whereas areas of intense development are found in classes 4 and 5. The maps were compared for the clarity of discrete urban features. An unsupervised classification may serve as support data for a more refined supervised classification. Based on a visual assessment of the unsupervised NDCCI/NBI/BAEI classification, classifying urban development in terms of low, medium, and high is straightforward, and further analysis was performed to create a refined classification with the SVM classifier by Cortes & Vapnik (1995).

Pal & Mather (2005) report success using SVM to classify Landsat 7 data for Littleport, England into eight cover types: wheat, water, dry salt lake, hydrophytic vegetation, vineyards, bare, pasture, and built-up. SVM draws upon statistical learning theory to identify decision boundaries to separate classes with an optimal hyperplane in feature space (Cortes & Vapnik, 1995; Pal & Mather, 2005). For linearly separable classes, SVM will identify the decision boundary that minimizes generalization error: the

one that leaves the greatest margin between the points, or "support vectors" of those classes closest to the hyperplane (Cortes & Vapnik, 1995; Pal & Mather, 2005). Classes that cannot be linearly separated are handled the same way, though the SVM performs a minimizing function handling the proportion of cells classified incorrectly (Cortes & Vapnik, 1995; Pal & Mather, 2005).

The NDCCI/NBI/BAEI composite was classified with pixel-based SVM with default settings, low-to-high, in terms of arbitrary classes named Urban 1-3 using training samples selected by comparing homogenous areas of the composite to high-resolution basemap imagery for 2016 available through ArcGIS. GML and Random Trees supervised classifiers were also applied with default settings, though they did not yield results that were comparable to SVM. Area statistics from the FDEP data were calculated to assess features typifying each class. It must be noted that the FDEP data covers Miami without breaks between features, which is advantageous since the SVM classification should correctly aggregate the entire city. NLCD Percent Developed Imperviousness data can be conditionally geoprocessed to select areas possessing a certain intensity of development (as defined by the USGS). That selection might then be fused with the SVM classification to maximize the amount of detail regarding urban intensity derived from a satellite image.

The USGS publishes NLCD, derived from Landsat data and delineating all land in the conterminous US into 21 classes, every five years. NLCD features four classes of urban intensity derived entirely from the NLCD Percent Developed Imperviousness

product, also released on the same five-year basis. The classes are Open Space, Low Intensity, Medium Intensity, and High Intensity. Open Space is typified by mostly vegetation (<20% impervious), Low Intensity by single-family homes (20-49% impervious), Medium Intensity by single-family homes (50-79%), and High Intensity by frequently traversed areas (80-100% impervious) (Jin et al., 2019).

NLCD urban intensities are based on groupings of developed surface imperviousness derived from satellite data, which physically limits the interpretation of feature structure. Furthermore, there are shortcomings such as fragments of Open Space incorrectly classified as Low Intensity, large patches of Low Intensity incorrectly classified as Open Space due to vegetation, High Intensity areas that are saturated and overflow into areas of lower intensity, and areas of high development incorrectly classified into the lower classes. Referring to **Figure 4**, the NLCD 2016 urban intensity map of Miami displays numerous noticeable errors; four examples are circled in yellow and numbered: 1) Fragments of Mount Nebo and Memorial Plan Flagler Memorial Parks incorrectly classified as Low Intensity, 2) A vegetated patch of the Coconut Grove neighborhoods incorrectly classified as Open Space, 3) An overflow of High Intensity along a commercial strip in the Little Havana neighborhood, 4) Marlins Park incorrectly classified in lower classes.

The SVM method identifies urban intensity in three simple classes and features corrections to class conflicts found in NLCD 2016. It was conditionally geoprocessed to increase detail by replacing any cells with an imperviousness between 50-79% with a

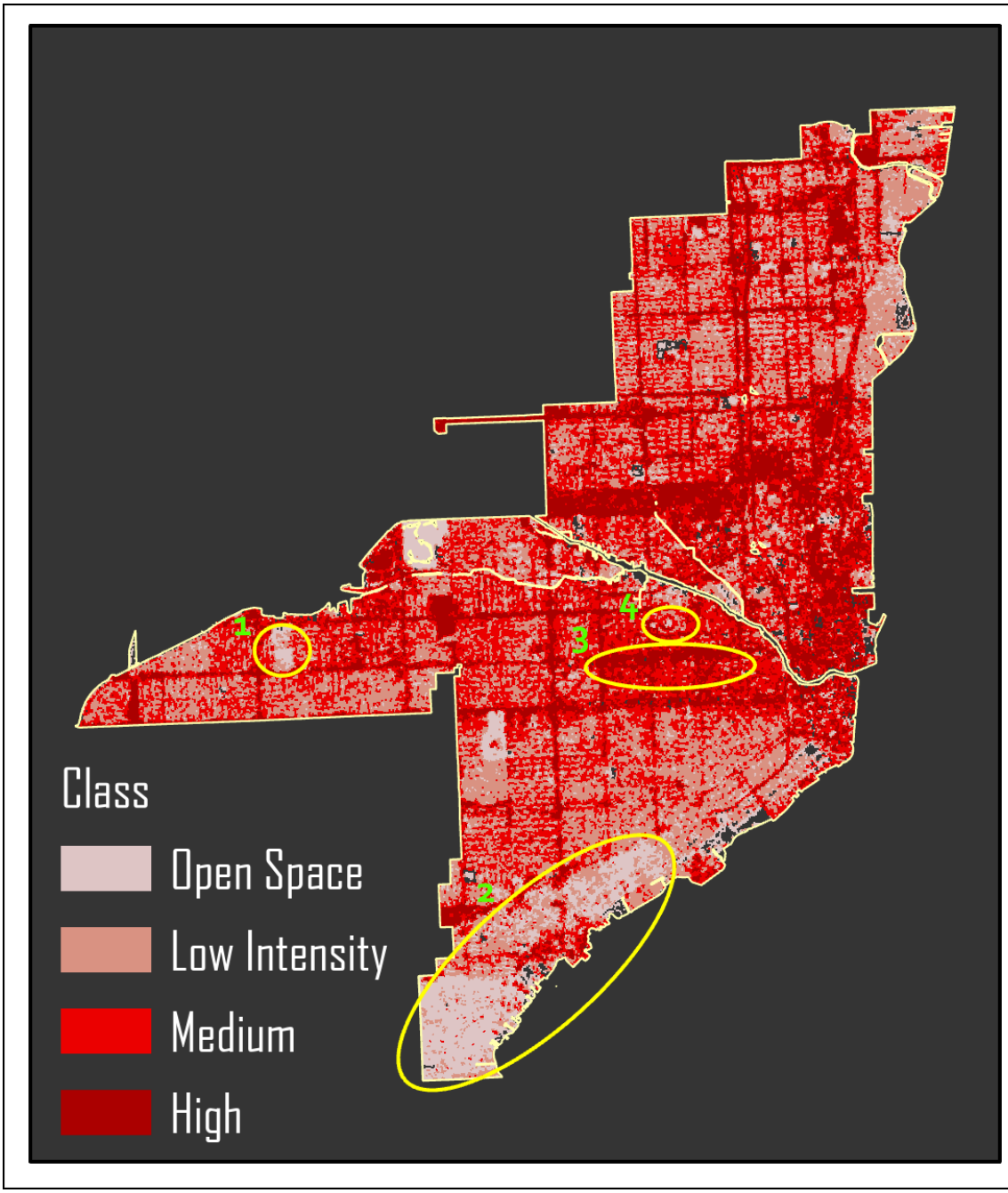

Figure 4. USGS NLCD 2016 urban intensities with noticeable errors denoted.

new class. The result of the SVM/Percent Developed Imperviousness fusion still displayed an incorrect classification for Marlins Park. It was revised with a conditional methodology to implement the Iso Cluster classification as a correction.

The SVM/Percent Developed Imperviousness fusion was conditionally geoprocessed to replace any cells classified as Urban 5 in the Iso Cluster classification with a new class. To finally amend the NLCD urban intensity classification, the fifth class was decomposed into the fourth. Area statistics were calculated from the FDEP data for the five-class and four-class maps to assess features that typify each class. Maps created for this part of the study were projected to the USA Contiguous Albers Equal Area Conic USGS coordinate system and resampled with cubic convolution to match the original NLCD products, which are distributed as cubic convolution maps in the Albers projection. The semi-automated workflow for creating the new urban LULC maps is summarized in **Figure 5**.

The urban land use classification methods introduced in this paper have the potential to serve as inputs into urban growth geosimulations. The next section will describe the creation of a geosimulation of the formation of high-rise infrastructure in the Brickell neighborhood incorporating BAEI as a shadow index.

2.6. Land Change Modeler

The LCM module of TerrSet can operate as a geostatistical Markov Chain predictor, utilizing the functionality of MLP ANN. LCM accepts input in the form of

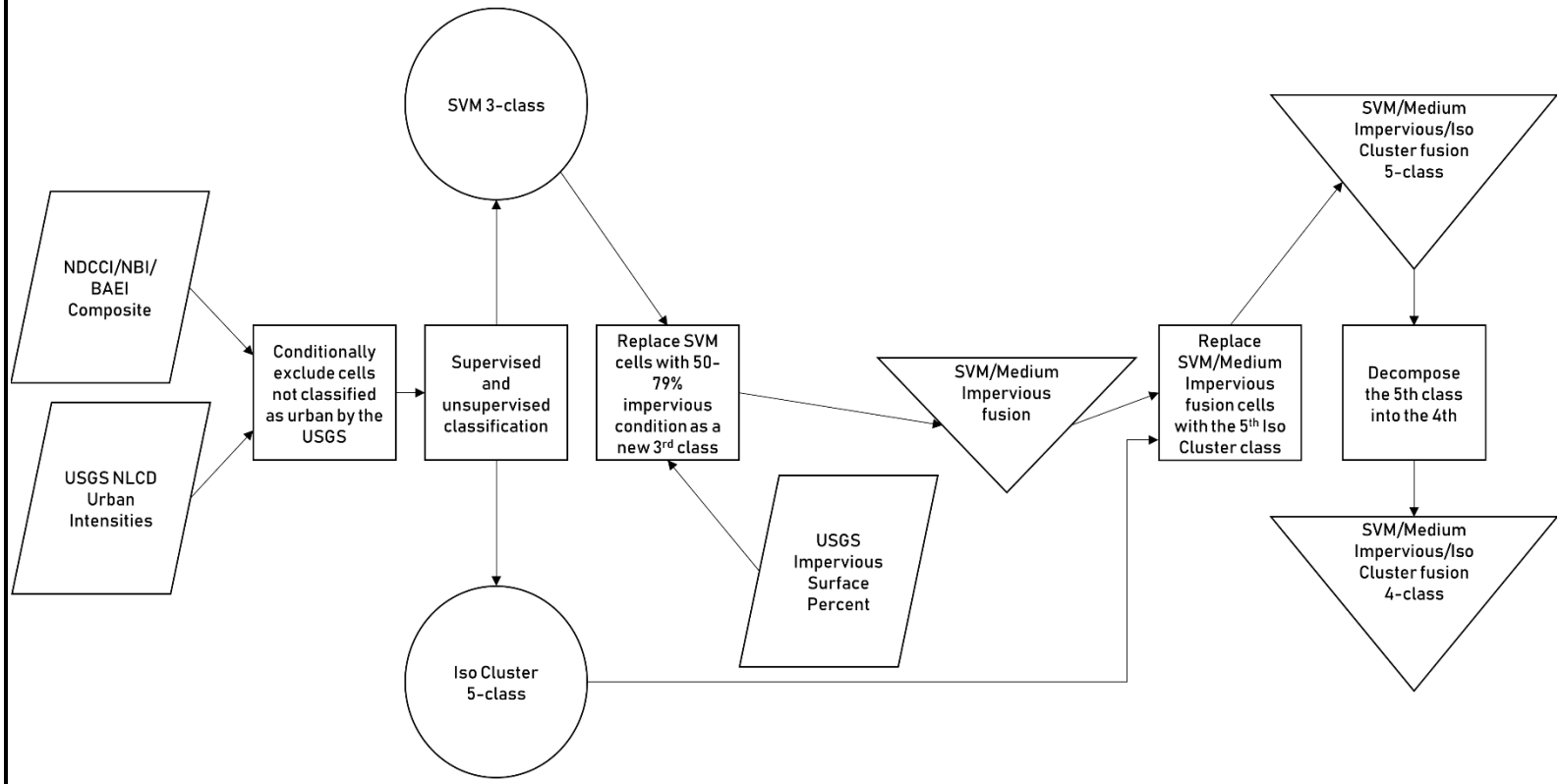

Figure 5. Urban intensity classification workflow diagram.

classified before-and-after rasters and predictor variables. Typical geographic predictors of urban development include elevation, distance to transportation, population, and income. In addition to these usual predictors, polynomial transition trends can be generated within the LCM module from the before-and-after data used to interpolate the prediction. Although geosimulations may have difficulty predicting the occurrence of isolated features as they appear over time, a novel method for predicting the growth of discrete urban features is evaluated (Guan et al., 2011; Rahimi, 2016; Sun et al., 2007).

A time-series of BAEI rasters without feature extraction thresholding, including data from Landsat 5 for 2003 and 2008 and Landsat 8 for 2016, clipped to the Brickell neighborhood, captures the formation of shadows. Additional clipping was performed to isolate an area of interest. By focalizing the rasters to a one-cell radius circle, the shadows were grouped into simple circular features in a new raster, and a threshold that set a good visible fit for highlighting the shadows seen in the BAEI images was applied. Then, simple four-class land use maps, compatible with the LCM module, were created for the 2003 and 2008 data through the manual interpretation of high-resolution 2016 basemap imagery available through ArcGIS. Class assignment was attributed to the polygons of a $30m^2$ vector fishnet which was rasterized and conditionally geoprocessed to include the shadows that overlap business areas. Before initiating the geosimulation, polynomial transition trends were mapped in LCM during the module's model fitting routine to determine a series of polynomial transition trends that could serve as effective predictors of the transition from "Business" to "High-rise Shadow." Only polynomial

transition trends were incorporated as predictors in this study. The assumption made was that the geosimulation need not predict the 2016 focalization exactly and that the prediction will, at least, closely outline the area where new high-rise infrastructure has been constructed. Default parameter settings, such as automatically assigned transition probabilities, were used for the model.

3. Results

3.1. The New Built-up Index

3.1.1. Zonal Statistics

Zonal statistics were calculated for discrete urban land use types for an NBI image derived from 2016 Landsat 8 OLI data (see **Table 2**). Statistically, there appeared to be pronounced differences in central tendency between the types listed. The mean values range from high, attributable to industrial land, down to commercial and institutional land, and down again to residential and recreational land. NBI arranges the brightness of urban surface features in linear order.

3.1.2. Object-oriented Image Analysis

Utilizing the mean shift between urban land use types, NBI can be segmented into object primitives. Primitives emphasizing brightness, shape, and texture were visualized in **Figure 6**, where the scaled values represent the brightness captured by each segment. Visual assessment of the primitives yields the idea that urban land use types can be identified as distinct objects. The properties of a segment extracted from should be cross-referenced with ground truth data to verify the usefulness of this methodology.

3.1.3. Feature Extraction

Table 2. Zonal statistics of NBI derived from 10/22/16 Landsat 8 OLI data, referencing FGDL land use data.

Land Use	Area (km²)	Min	Max	Range	Mean	Std
Centrally Assessed[1]	0.33	0.0195	0.2788	0.2593	0.1262	0.0535
Industrial	1.97	0.0209	0.5135	0.4927	0.1698	0.0663
Institutional[2]	2.51	0.0002	0.4243	0.4241	0.0846	0.0639
Public/Semi-public[3]	7.99	0.0004	0.7474	0.7470	0.0931	0.0711
Recreation	0.6	0.0037	0.3645	0.3607	0.0631	0.0564
Residential	36.78	0.0004	0.4011	0.4008	0.0785	0.0421
Retail/Office	7.52	0.0044	0.7848	0.7804	0.1356	0.0701
Vacant Non-residential	2.61	0.0056	0.4932	0.4877	0.1120	0.0754
Vacant Residential	1.84	0.0035	0.2860	0.2825	0.0607	0.0449

A single object was extracted from NBI by vectorizing a segment created with a spectral detail of 15.5, a spatial detail of 15, and a minimum segment size of 1000 (see **Figure 7**). The feature was selected based on a visual assessment of the brightness and configuration of surface features. According to zonal statistics referencing FGDL land use data, the object is typified by the presence of industrial and commercial land use (see **Table 3**). NBI is useful in the process of OBIA for the identification and potential classification of urban land use types.

3.2. The Built-up Area Extraction Index

3.2.1. Change Detection

Visual and statistical analysis was made of a BAEI time-series, including data from Landsat 5, Landsat 7, and Landsat 8, for the entire city (see **Figure 8**). The time-

[1] For instance, utilities.
[2] Religious, educational, social, cultural, healthcare.
[3] Schools, governmental.

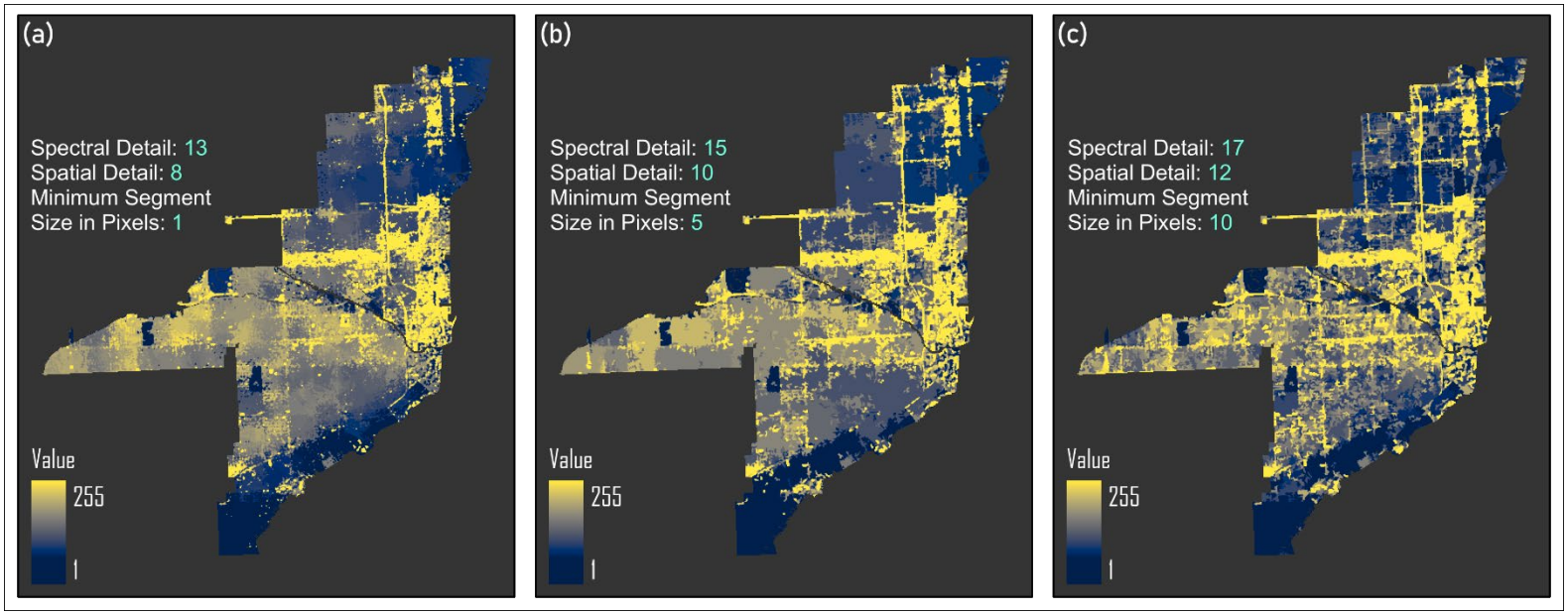

Figure 6. NBI object primitives derived from Landsat 8 OLI 10/22/16 data; (a) small segment size emphasizing surface brightness, (b) moderate segment size emphasizing surface objects, (c) large segment size emphasizing surface texture.

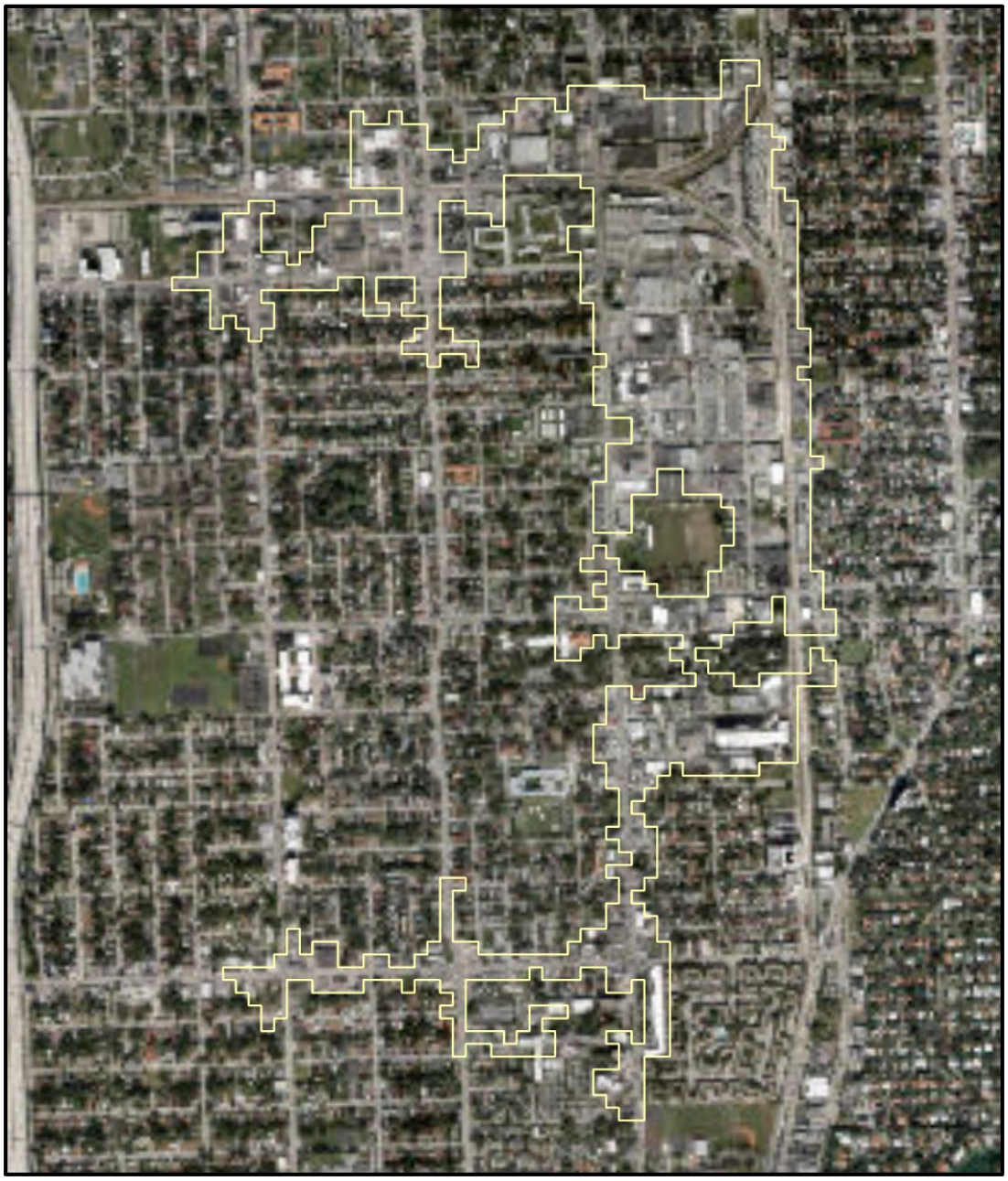

Figure 7. NBI-derived object encompassing industrialized land in the Little Haiti neighborhood.

Table 3. Area statistics of NBI-derived object, referencing FGDL data.

Land Use	Area (km²)
Centrally Assessed	0.06
Industrial	0.43
Institutional	0.05
Public/Semi-public	0.04
Residential	0.03
Retail/Office	0.14
Vacant Nonresidential	0.05

series corresponds with a population influx and subsequent accumulation of low-albedo construction materials due to human development. There appears to be a trend of increasing central tendency for the Landsat 5 and 7 data. Image comparison was performed between the Landsat 8 data, and they also show an increase in central tendency despite the small, two-year time frame between them.

3.2.2. Change Detection II

A similar time-series analysis, comparing BAEI to NDVI, was conducted with the Landsat 5 data for part of Miami truncated of neighborhoods with developed urban canopies to minimize the influence of vegetation on BAEI returns (see **Figure 9**). The BAEI time-series possesses an increasing mean, while the NDVI mean is decreasing. There is a clear, continual increase in the central tendency of BAEI for areas not shrouded by urban canopy. Moreover, zonal statistics were calculated for the truncated study area with a time-series of ten images spanning 1985-2016, including data from

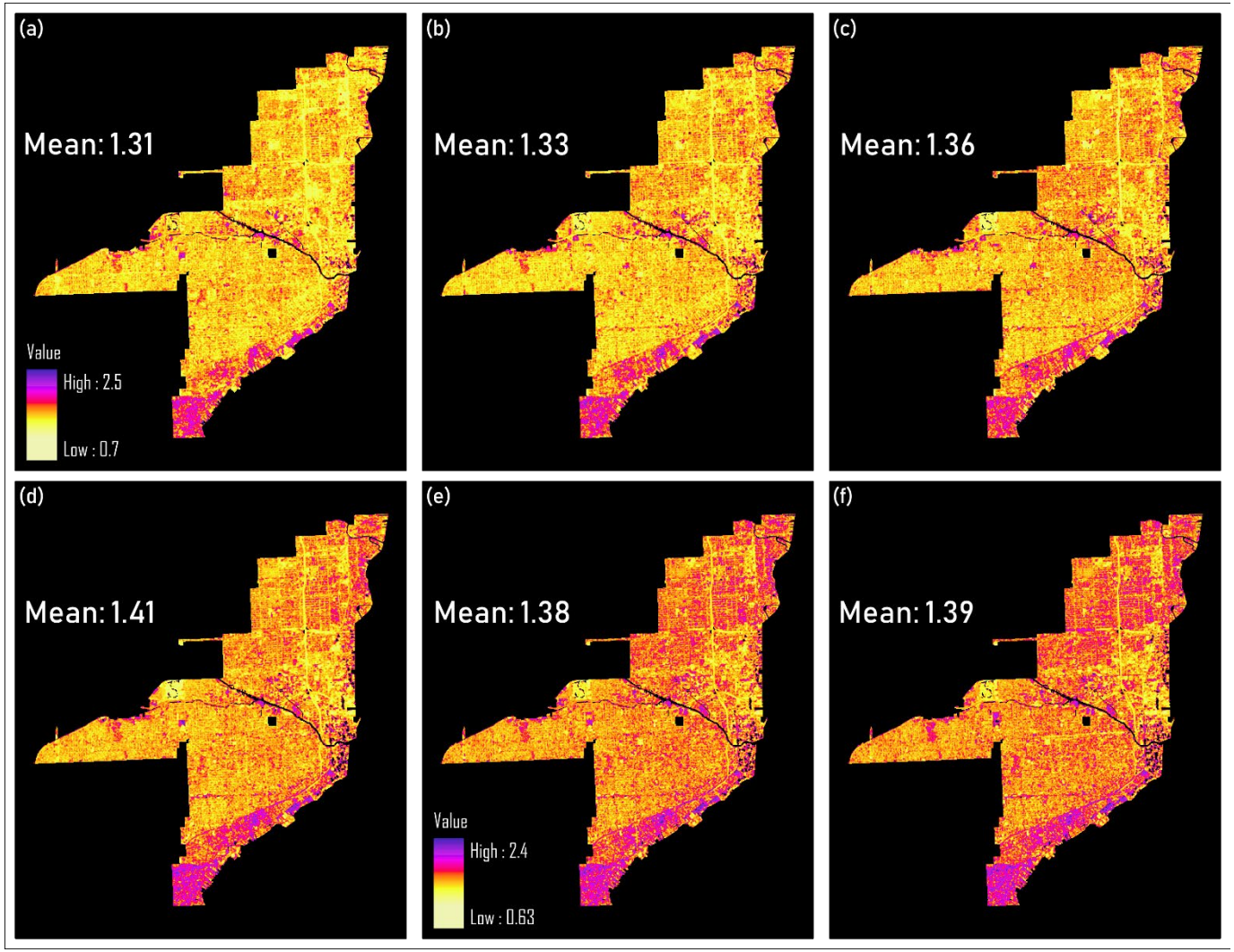

Figure 8. BAEI change detection time-series, giving mean index values, derived from Landsat data; (a) 5 TM 11/02/85, (b) 11/06/98, (c) 11/10/11, (d) 7 ETM+ 02/05/00, (e) 8 OLI 10/17/14, (f) 10/22/16.

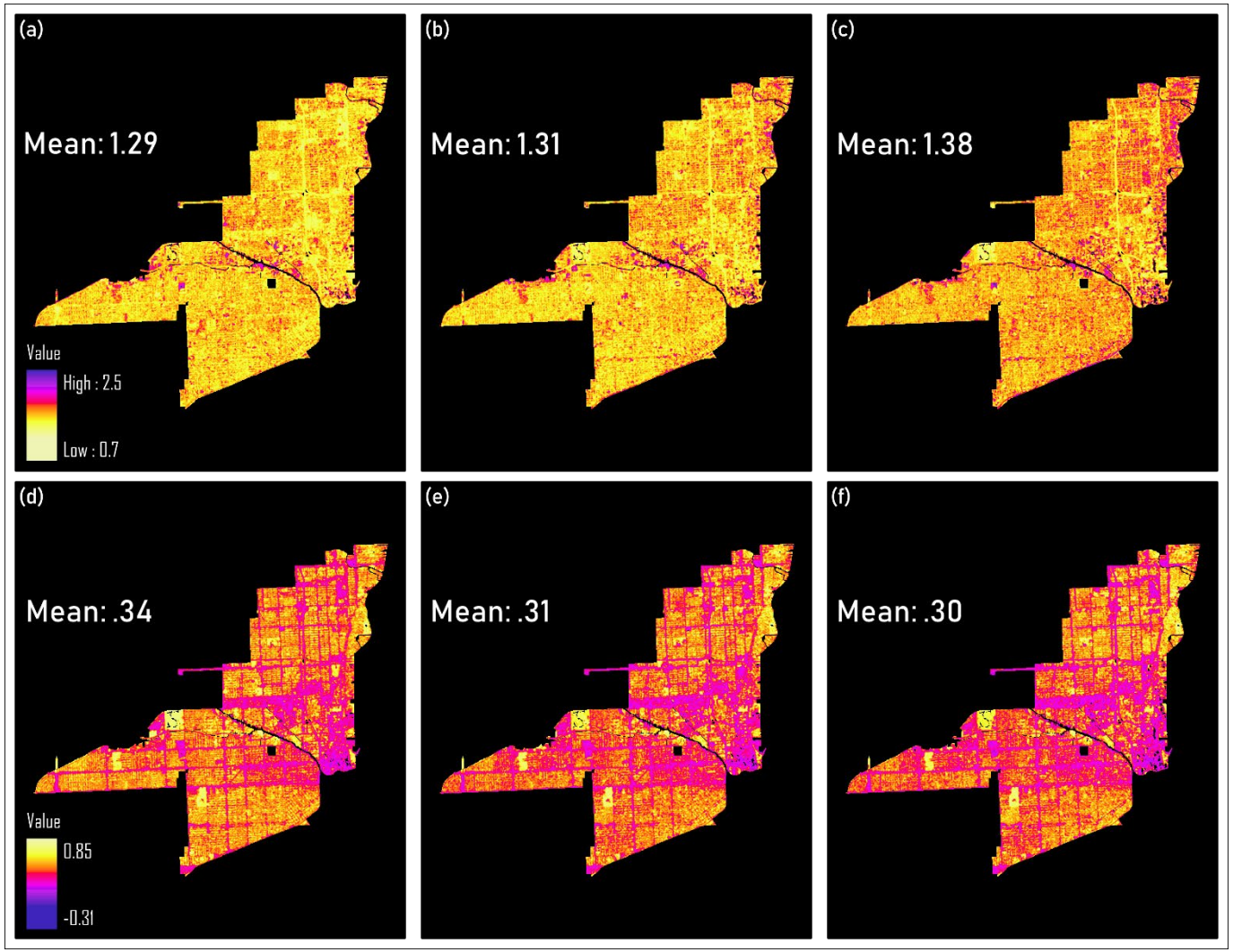

Figure 9: Change detection time-series for the truncated study area, giving mean index values, derived from Landsat 5 TM data; (a) 11/02/85 BAEI, (b) 11/06/98 BAEI, (c) 11/10/11 BAEI, (d) 11/02/85 NDVI, (e) 11/06/98 NDVI, (f) 11/10/11 NDVI.

Landsat 5, 7, and 8. **Table 4** displays a trend of increasing BAEI values corresponding with decreasing NDVI values, indicating a negative correlation.

Table 4. Zonal statistics of BAEI and NDVI values derived from Landsat 5 TM (1985-1998 & 2003-2011), 7 ETM+ (2000), and 8 OLI data (2014 & 2016), referencing the truncated study area.

Year	Mean BAEI	Mean NDVI
1985	1.283	0.3388
1998	1.304	0.3121
1999	1.284	0.3142
2000	1.338	0.2733
2003	1.332	0.3074
2008	1.364	0.2945
2009	1.299	0.2891
2011	1.377	0.3049
2014	1.353	0.3900
2016	1.367	0.3897

3.3. The Normalized Difference Concrete Condition Index

Building on the measurements achieved with NBI and BAEI, enhancements can be composited into a stack that could be utilized for the creation of discrete urban classes (Ettehadi et al., 2019). Miami's urban fabric is rendered with NDCCI as a pronounced network of streets within open space, residential, and business areas. An effective enhancement composite would emphasize differences that exist between features within an urban landscape, where NBI, BAEI, and NDCCI do not yield similar renderings.

Since NDVI is useful for identifying areas with or without vegetation, zonal statistics were derived from urban land use types for both NDCCI and NDVI, both derived from 2016 Landsat 8 data. NDCCI possesses less variation within classes,

according to the coefficient of variation (CV) statistic, compared to NDVI (see **Tables 5a and 5b**). CV is calculated by dividing the standard deviation by the mean; it gives a measure of the amount of statistical variation that exists between classes, allowing for direct comparison.

Table 5a. Zonal statistics of 10/22/16 NDCCI, referencing FGDL data.

Land Use	Area (km²)	Min	Max	Range	Mean	Std	CV
Centrally Assessed	0.33	0.004	0.701	0.698	0.345	0.124	35.96%
Industrial	1.97	-0.100	0.649	0.749	0.221	0.106	47.96%
Institutional	2.51	-0.316	0.881	1.197	0.461	0.190	41.12%
Public/Semi-public	7.99	-0.136	0.914	1.050	0.439	0.189	42.93%
Recreation	0.6	-0.177	0.824	1.002	0.515	0.208	40.33%
Residential	36.78	-0.289	0.915	1.205	0.481	0.138	28.61%
Retail/Office	7.52	-0.811	0.886	1.697	0.262	0.141	53.98%
Vacant Non-residential	2.61	-0.462	0.827	1.289	0.392	0.186	47.42%
Vacant Residential	1.84	-0.185	0.845	1.030	0.535	0.172	32.18%

Table 5b. Zonal statistics of 10/22/16 NDVI, referencing FGDL data.

Land Use	Area (km²)	Min	Max	Range	Mean	Std	CV
Centrally Assessed	0.33	0.014	0.785	0.771	0.322	0.148	45.80%
Industrial	1.97	-0.065	0.699	0.764	0.185	0.112	60.48%
Institutional	2.51	-0.217	0.955	1.171	0.463	0.229	49.45%
Public/Semi-public	7.99	-0.057	0.972	1.029	0.442	0.225	51.03%
Recreation	0.6	-0.081	0.904	0.985	0.536	0.247	46%
Residential	36.78	-0.123	0.958	1.081	0.461	0.162	35.21%
Retail/Office	7.52	-0.633	0.944	1.576	0.234	0.153	65.41%
Vacant Non-residential	2.61	-0.296	0.905	1.201	0.384	0.220	57.31%
Vacant Residential	1.84	-0.117	0.925	1.042	0.550	0.207	37.60%

3.4. Three-enhancement Composite

3.4.1. Iso Cluster

The possibility of mapping by compositing the three enhancements discussed above was also investigated. Iso Cluster classifications for NDCCI/NBI/BAEI and NDVI/NBI/BAEI composites were created for visual comparison. The default ArcGIS Iso Cluster settings are Maximum Number of Classes: 5, Maximum Number of Iterations: 20, Maximum Number of Cluster Merges per Iteration: 5, Maximum Merge Distance: 0.5, Minimum Samples Per Cluster: 20, and Skip Factor: 10. These settings were not changed. Both composites were assigned arbitrary classes of Urban 1-5. The default analysis settings are Maximum Number of Classes: 5, Maximum Number of Iterations: 20, Maximum Number of Cluster Merges per Iteration: 5, Maximum Merge Distance: 0.5, Minimum Samples Per Cluster: 20, and Skip Factor: 10. These settings are not changed. Both composites are assigned arbitrary classes of Urban 1-5, yielding a view of development intensities based on respective enhancements. Examining the two maps in **Figure 10**, finer surface features such as Marlins Park, highways, and streets are more vividly rendered with the NDCCI/NBI/BAEI classification. The features in the NDVI/NBI/BAEI are comparatively saturated, yielding a compromise of less detail. Therefore, further analysis was conducted with a supervised classifier to map the spatial configuration of Miami's urban features more accurately.

3.4.2. Support Vector Machine

A supervised classification was created with the SVM classifier to build upon the unsupervised classification of the NDCCI/NBI/BAEI composite. The default analysis

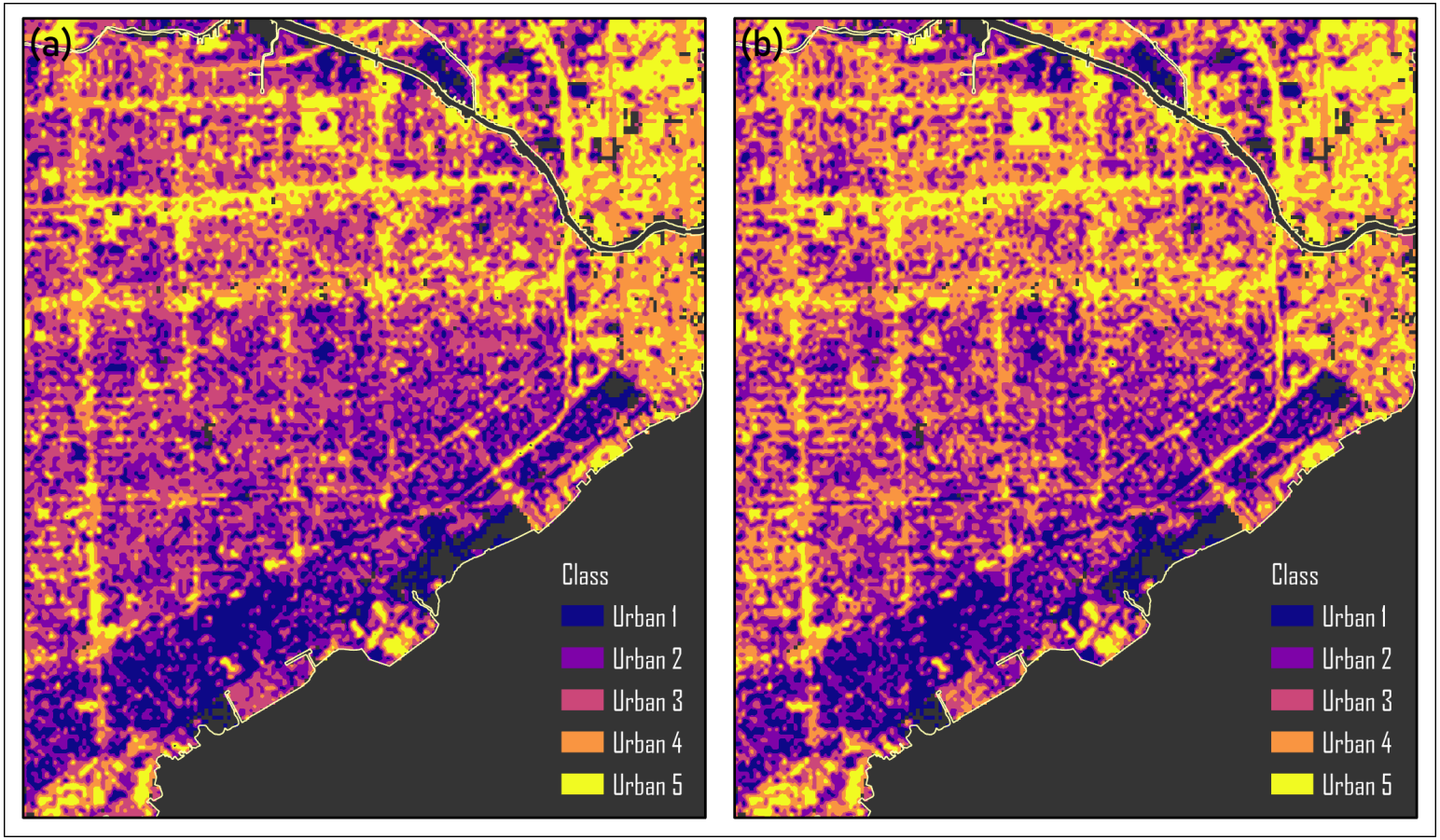

Figure 10. Iso Cluster classifications of urban land use intensity based on spectral index composites derived from 10/22/16 Landsat 8 OLI data; (a) NDCCI/NBI/BAEI composite, (b) NDVI/NBI/BAEI composite.

setting of Maximum Number of Samples per Class: 500, was not changed. Training samples were established to separate open space, residential and vegetated residential, and business and transport areas into classes Urban 1-3, indicating the intensity of development (see **Figure 11a**). Zonal statistics were calculated for urban land use types to assess the accuracy of the SVM classification. Referring to **Table 6**, Urban 1 is typified by recreation and other low-intensity development, Urban 2 by residential areas, and Urban 3 by business and other high-intensity development. Where NLCD features an additional class to describe Medium Intensity, further analysis was conducted to fuse that class with the SVM classification to increase cartographic detail.

3.4.3. NLCD Percent Developed Imperviousness

USGS classifies areas identified as possessing 50-79% impervious surface as Medium Intensity, and the class is rendered as a detail of streets and well-developed buildings in the NLCD classified product. The SVM classification reduces the errors related to feature structure found in NLCD 2016. In reciprocal, areas identified by USGS as 50-79% impervious were conditionally geoprocessed to overlay the SVM classification as a new third class, yielding classes Urban 1-4 (see **Figures 11b & 11c**).

3.4.4. The Fusion Map

Upon visual inspection, it was discerned that some well-developed features, such as Marlins Park, may still be classified incorrectly into lower classes after fusing the

SVM classification with the NLCD Percent Developed Imperviousness. To correct those features, the fifth class of the unsupervised NDCCI/NBI/BAEI classification was overlaid as a new class. Upon subsequent visual inspection, the result of adding this fifth class was a successful fusion; the brightest features were classified as Urban 5. By decomposing the fifth class into the fourth, a new four-class urban intensity map without the pronounced errors of NLCD 2016 was created (see **Figures 11d-11f**).

Zonal statistics were calculated for the NLCD 2016 Miami urban intensities and the NDCCI/NBI/BAEI five-class and four-class fusion maps. Improvements were made in the fusion classifications (see **Tables 7a-7c**). For example, NLCD 2016 Open Space is typified by both open areas and urban canopy, and the refined fusion classification effectively separates open areas from the urban canopy. The distribution of urban intensity classes among land use types is similar between the four-class maps. However, NLCD 2016 shows a large amount of residential areas classified incorrectly in the first class. Also, NLCD 2016 shows noticeably less area in the fourth class. Having established mapping conventions with NBI, BAEI, and NDCCI, further consideration was given to the potential for establishing an infill urban growth prediction implementing well-known land change geosimulation modeling methodology based on the unexplored potential of utilizing the BAEI as a shadow index.

3.5. Multilayer Perceptron Artificial Neural Network Geosimulation

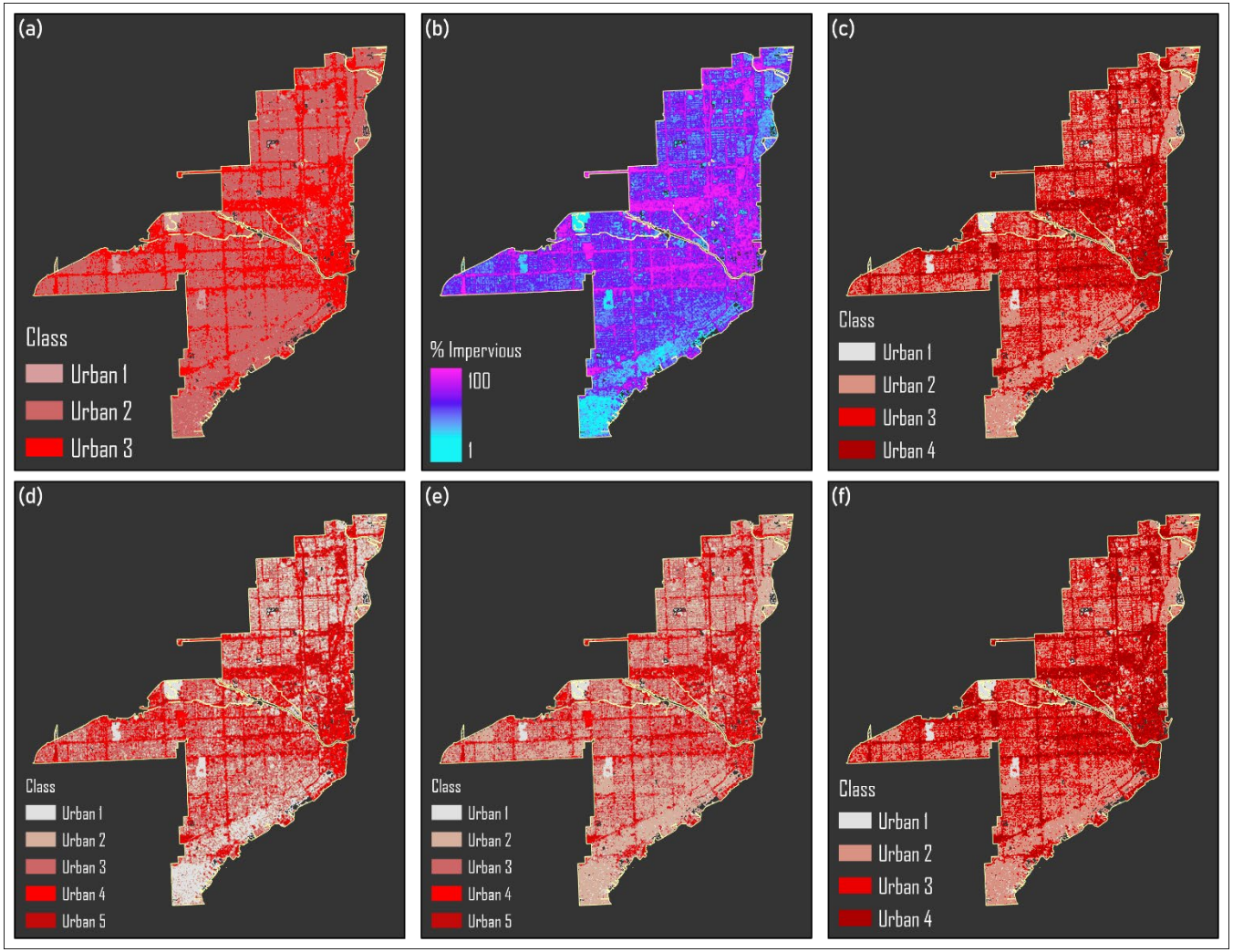

Figure 11. 2016 Miami urban land use classifications derived from Landsat 8 OLI data; (a) NDCCI/NBI/BAEI composite SVM, (b) NLCD 2016 % Developed Imperviousness, (c) fusion of NDCCI/NBI/BAEI SVM and % Developed Imperviousness, (d) NDCCI/NBI/BAEI composite Iso Cluster, (e) five-class fusion of % Developed Imperviousness with NDCCI/NBI/BAEI SVM and Iso Cluster, (f) four-class fusion of % Developed Imperviousness with NDCCI/NBI/BAEI SVM and Iso Cluster.

Table 6. Area statistics for SVM classification of NDCCI/NBI/BAEI composite derived from 10/22/16 Landsat 8 OLI data, referencing FDEP data.

Land Use	Urban 1 (km²)	Urban 2	Urban 3
Commercial and Services	0.630	3.480	10.886
Industrial	0.027	0.460	2.651
Institutional	0.390	2.156	1.989
Open Land	0.054	0.070	0.098
Recreational	0.736	0.671	0.494
Residential High Density	0.260	5.098	4.091
Residential Low Density	0.010	0.065	0.000
Residential Medium Density	1.326	40.167	5.099
Transportation	0.049	0.854	2.095
Utilities	0.004	0.044	0.138

Table 7a. Area statistics of USGS NLCD 2016 urban land use classification, referencing FDEP data.

Land Use	Open Space (km²)	Low	Medium	High
Commercial and Services	0.546	1.434	5.171	7.932
Industrial	0.008	0.109	0.663	2.367
Institutional	0.457	1.047	1.932	1.112
Open Land	0.033	0.094	0.077	0.022
Recreational	0.795	0.504	0.434	0.179
Residential High Density	0.320	2.218	4.984	1.967
Residential Low Density	0.043	0.032	0.002	0.000
Residential Medium Density	5.084	22.002	17.768	1.861
Transportation	0.111	0.444	1.179	1.288
Utilities	0.000	0.017	0.055	0.113

Table 7b. Area statistics of five-class fusion of 2016 impervious surface fraction with NDCCI/NBI/BAEI SVM and Iso Cluster urban land use classifications, referencing FDEP data.

Land Use	Urban 1 (km²)	Urban 2	Urban 3	Urban 4	Urban 5
Commercial and Services	0.560	1.694	4.271	4.210	4.163
Industrial	0.020	0.252	0.502	0.916	1.440
Institutional	0.330	1.162	1.645	0.630	0.717
Open Land	0.048	0.041	0.058	0.028	0.046
Recreational	0.669	0.446	0.330	0.170	0.206
Residential High Density	0.209	2.221	4.577	1.434	0.970
Residential Low Density	0.009	0.059	0.002	0.000	0.000
Residential Medium Density	1.204	25.489	17.027	1.526	1.189
Transportation	0.041	0.455	0.888	0.500	1.083
Utilities	0.003	0.022	0.041	0.052	0.068

Table 7c. Area statistics of four-class fusion of 2016 impervious surface fraction with NDCCI/NBI/BAEI SVM and Iso Cluster urban land use classifications, referencing FDEP data.

Land Use	Urban 1 (km²)	Urban 2	Urban 3	Urban 4
Commercial and Services	0.560	1.694	4.271	8.374
Industrial	0.020	0.252	0.502	2.356
Institutional	0.330	1.162	1.645	1.347
Open Land	0.048	0.041	0.058	0.074
Recreational	0.669	0.446	0.330	0.376
Residential High Density	0.209	2.221	4.577	2.404
Residential Low Density	0.009	0.059	0.002	0.000
Residential Medium Density	1.204	25.489	17.027	2.715
Transportation	0.041	0.455	0.888	1.583
Utilities	0.003	0.022	0.041	0.120

3.5.1. Geosimulation Inputs: BAEI as a Shadow Index

BAEI was calculated using Landsat 5 data for 2003 and 2008, and Landsat 8 data for 2016 was clipped to the Brickell neighborhood. Without a conditional threshold, the shadows cast by high-rise infrastructure were rendered clearly in higher BAEI values. The output rasters were clipped to an area of interest where shadows seem to be developing over a time-series for visualization. By focalizing the BAEI rasters with a one-cell radius, the formation of shadows was highlighted by a group of high values. Each focalization was then conditionally thresholded to assign 1 to areas with high values, indicating the presence of shadows, and 0 to areas with low values and symbolized with transparency over rasters symbolized with a standard deviation stretch and gamma adjustments (see **Figure 12**). Upon visual inspection, it was assumed that attempting to predict the area highlighted in the 2016 data, by referring to the 2003 and 2008 images, would be best approached by attempting to generalize the prediction by

"circling" the area.

For the 2003 and 2008 data, manual classifications were performed for the Brickell neighborhood, assigning each $30m^2$ cell to either Road, Low Development, or Business classes. Conditional focalizations created for Brickell were then integrated into the manual classifications to create maps depicting the formation of shadows for each year in the time-series. These maps were used as inputs to the TerrSet LCM module. From the input maps, LCM can automatically calculate polynomial transition trends for use as predictor gradients in the geosimulation. During the LCM model fitting routine, where the predictive capacity of every combination of polynomial trends can be examined, 2nd and 3rd order polynomial transition trend maps were selected as best fit predictors for the visualization (see **Figure 13**).

3.5.2. Geosimulation Output: Projected Vector

The geosimulation was executed with default settings. LCM features an accuracy assessment tool that will accept a classification map as input, though the results of this analysis were left to visual assessment. The output raster was clipped to the area of interest and vectorized. **Figure 14** displays the geosimulation output as two maps: the predicted land use classification for the area of interest and a simplified vector of the output classified as shadows. The predicted vector referencing the 2016 data provides a visual fit for the shadows rendered in BAEI.

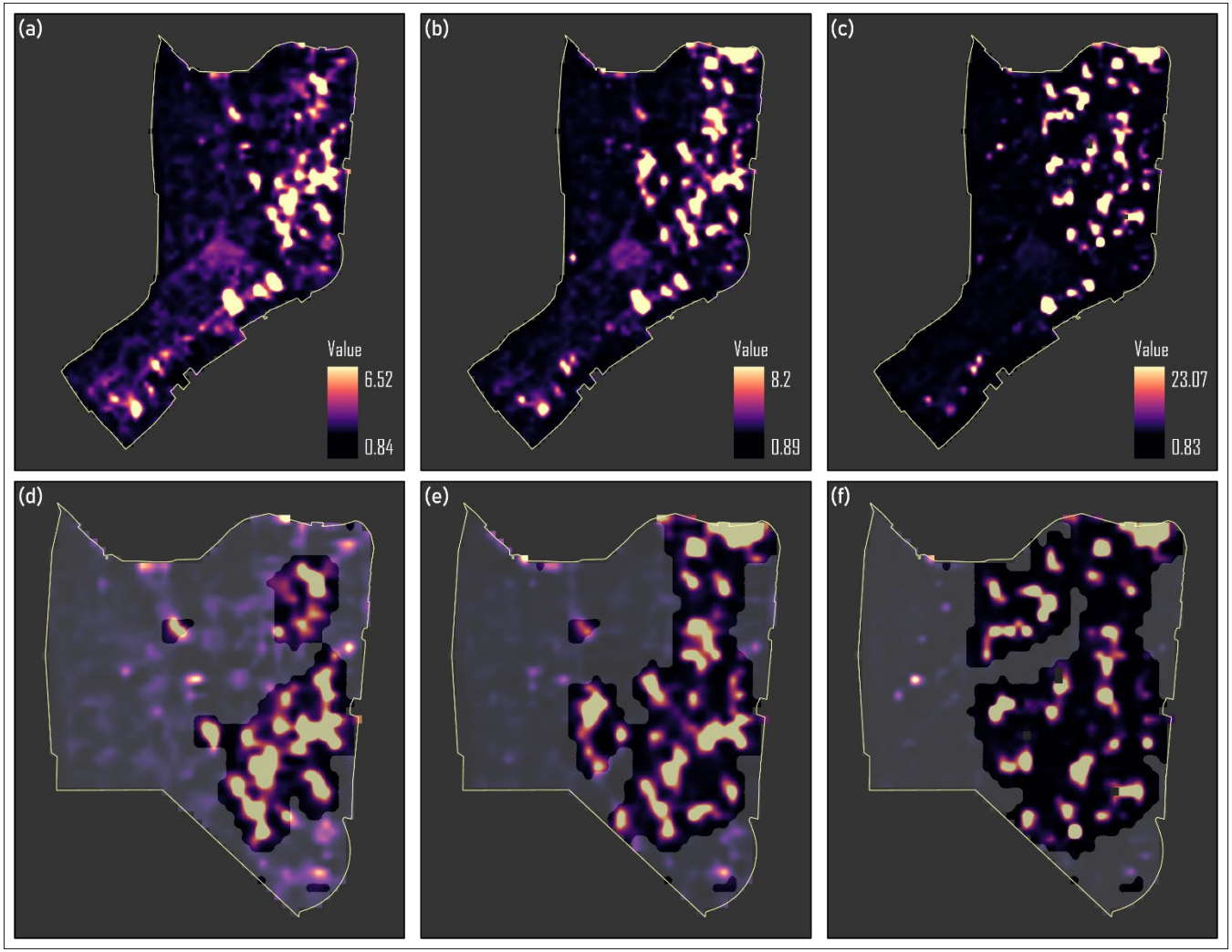

Figure 12. BAEI (as a shadow index) change detection time-series of the Brickell neighborhood derived from Landsat data; (a) 5 TM 11/20/03, (b) 11/17/08, (c) 8 OLI 10/22/16. The area of interest overlaid with a focalized classification (transparent) based on thresholding; (d) 5 TM 11/20/03. (e) 11/17/08. (f) 8 OLI 10/22/16.

Figure 13. Classifications, created by manual and semi-automated methods, of the Brickell neighborhood derived from Landsat 5 TM data used as LCM inputs; (a) 11/20/03, (b) 11/17/08. Polynomial transition trends created in LCM; (c) 2nd order, (d) 3rd order.

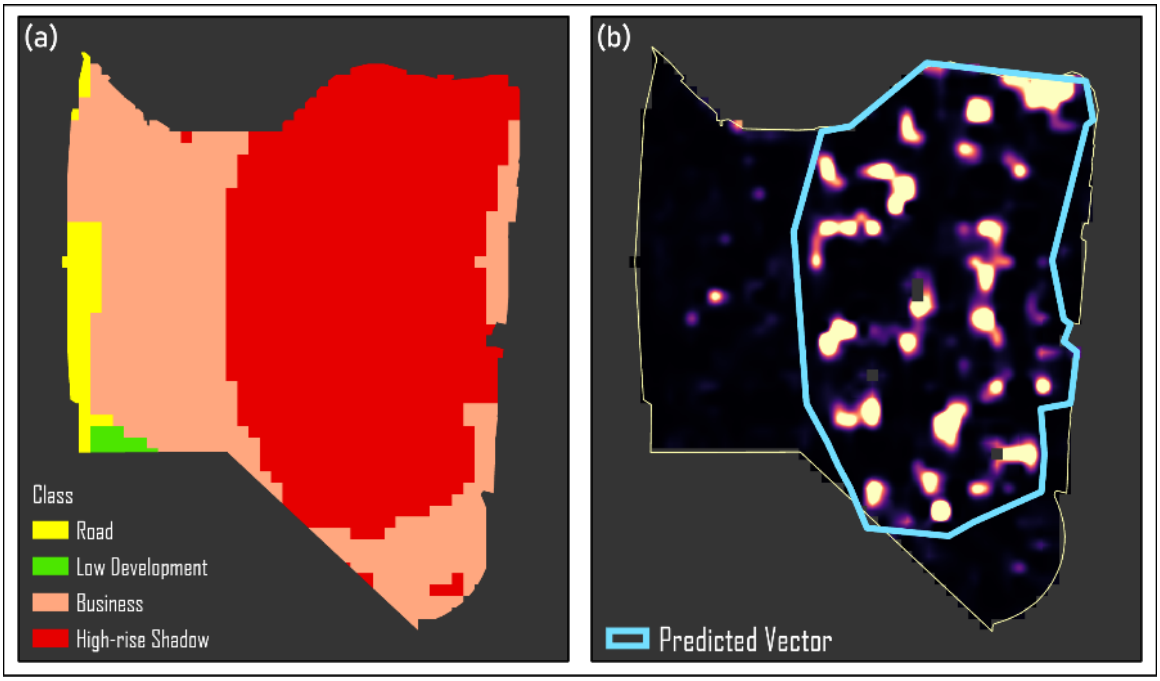

Figure 14. Results of LCM MLP 2016 prediction for Brickell neighborhood area of interest based on 2003 and 2008 data; (a) predicted 2016 area of interest land cover, (b) vector derived from 2016 prediction referencing the formation of shadows in the area of interest.

4. Discussion

Jieli et al. (2010) developed NBI to enhance the scale of the brightness of urban features in a satellite image. Value ranges for NBI calculated from 2016 Landsat 8 data are found to be descriptive of discrete land use types, according to feature brightness. Objects emphasizing the shape of Miami's urban feature types were visualized, and an object delineating an isolated formation of industrial land was successfully extracted. Through OBIA, it is possible to create maps that display urban land use as a series of classified geometries. Such methodology may entail automated geoprocessing of a large series of object settings, and the output rasters can then be reviewed by an operator to select the most fitting segments as shapes to map the target urban area. It is proposed that NBI be utilized for feature extraction of urban land use types.

Building upon the potential for identifying discrete urban land use types with NBI, the possibility of grading urbanization in terms of collective building presence was investigated. Bouzekri et al. (2015) developed BAEI to enhance the brightness of urban features in a satellite image. Time-series analyses of Miami visualized with BAEI spanning 1985-2016 yields a view of linear increase. Visual comparison with NDVI, when the study area was truncated of neighborhoods possessing pronounced urban canopy, indicates that BAEI is more useful for tracking shifts in urban morphology. Also, the success of a 10-image time-series analysis comparing BAEI and NDVI for the truncated area was successful in identifying a negative correlation between the two indices. This suggests that BAEI is useful for measuring the extent of large-scale

urbanization as a low-high gradient, while NDVI is useful for measuring the vigor of plants. It is proposed that BAEI may be utilized during urban surface quality analyses to describe the upward scale of development.

Samsudin et al. (2016) developed NDCCI to enhance the presence and condition of construction material. Therefore, despite similar spectral configurations, it was suggested that NDCCI might be more useful for urban mapping than NDVI, which is designed to enhance the presence and condition of vegetation. A comparison between NDCCI and NDVI, derived from 2016 Landsat 8 data, with FGDL Miami land use data found NDCCI possesses less within-class variance compared to NDVI. Additionally, a visual comparison of Iso Cluster classifications of 2016 NDCCI/NBI/BAEI and NDVI/NBI/BAEI composites showed the NDCCI composite rendered Miami with less saturation between features of various intensity. Unsupervised classification yields maps that, by themselves, may be valuable for the identification of specific surface features and for vectorizing those features into point, polygon, or line shapes.

Furthermore, it was discernable that urbanization can be linearly rendered according to three dominant feature types: open space, residential, and business/transport areas. Therefore, SVM was used to classify the NDCCI composite in three stages of intensity based on training samples derived from a comparison between the composite and 2016 high-resolution satellite imagery. The success of this method can be replicated globally to provide urban LULC maps that describe development in three classes. In addition to functioning as a stand-alone method, it serves as a palette for more detailed

cartographic analyses to maximize the amount of information extracted from satellite data.

It was possible to add more detail by fusing the SVM classification with the NLCD Percent Developed Imperviousness product. The area of Miami classified in NLCD 2016 as Medium Intensity was fused with the SVM classification, in addition to the fifth class of the NDCCI composite Iso Cluster classification to correct any residual errors. The five-class fusion map does much to divide areas of the highest intensity from the fourth class, and the visualization may possess an aesthetic appeal. The four-class fusion map is more homogenous compared to NLCD 2016, having misclassification errors associated with urban intensities derived only from the Percent Developed Imperviousness corrected.

It is proposed that the process of classifying urban intensity with a satellite image in this analysis is effective for creating cartographic products of urban intensity that are superior to those currently found in NLCD. Because of the automated workflow, it is within reason to assert this methodology, when rigorously applied, may facilitate the production of maps on any scale. Challenges include the availability of remotely sensed data, fitting the Iso Cluster classification to suitably capture the intensity of features, and the establishment of correct training samples when using SVM. While the Iso Cluster and SVM maps can be generated globally, it is understood that the fusion maps can only be generated if a developed surface imperviousness product exists for the area being mapped.

There is global consideration for the use of LULC maps, such as those created during this research, as inputs into predictive geosimulations (Guan et al., 2011; Rahimi, 2016; Sun et al. 2007). For example, Sun et al. (2007) simulate the internal growth of Calgary, Alberta, Canada utilizing discrete classes derived from city land use data. Object maps derived from NBI may be implemented to facilitate this type of geostatistical modeling. In this study, BAEI rasters without feature extraction thresholds were focalized to magnify the presence of high-rise shadows detected in Miami's Brickell neighborhood. Classifications derived from manual interpretation and focal analysis of 2003 and 2008 Landsat 5 data were used as inputs for an MLP ANN Markov Chain geosimulation, in addition to polynomial transition trends derived from the classifications for predictors. The geosimulation generated a land use prediction that closely circled the formation of high-rise shadows in 2016 Landsat 8 data.

Additional model fitting may be useful in refining a prediction, such as the implementation of other predictor gradients. It is proposed that this is a novel method for simulating the formation of skyscrapers based on the reasonable fit of the projected vector, and that this analysis serves as a basic example of effective modeling that can be achieved through the proper model fitting of the LCM module. The proposed methodology may be replicated to predict the formation of any relevant discrete occurrence that may be otherwise difficult to predict, given the isolated nature of the occurrence.

5. Conclusion

Rapid urbanization stimulates a high demand for static mapping and geosimulations to support legislative and planning purposes. A caveat exists where LULC maps should be synthesized through a process of maximizing the amount of information that can be acquired from a satellite image. While this is not the first study to research the potential for incorporating spectral enhancements in classification processes delineating multiple states of urbanization, the paper systematically summarizes specific approaches to various aspects of urban analysis. It discusses the advantages and limitations of existing indices. The power of remote sensing and GIS were coupled to conceptualize new urban land use classification capabilities utilizing the NBI, BAEI, and NDCCI spectral enhancements. LULC maps generated without the details that may be acquired from these enhancements may be less useful in application.

Today, the trend of global urbanization has negatively impacted Earth with climate change, lowering water quality, and reducing natural landscape, among other problems. In response, there is an increased need for frequently updated LULC maps, and smart growth policies have been implemented by those responsible for managing the development of cityscapes. The principle of infill development, the redevelopment of land within a cityscape, will become more important because of the goal of smart growth policies to build compact, high population urban areas instead of sprawling outward. When combined with the analytical capabilities of GIS, remote sensing data may be refined to focus on a specific geography. Miami, a city that exists in a sensitive coastal

environment, continues to grow at a rapid pace. We should consider using the city as a study area for research on urban geographic information science. Maps derived from this research may be advantageous for strengthening all purposes that rely on LULC maps.

Significant to this study, NBI was demonstrated to possess the unique property of identifying discrete urban land use types as segmented objects. Urban LULC maps may be created, through the process of OBIA, based on the geometric configuration of discrete land use types rendered in NBI. BAEI was successfully implemented to visualize and scale the growth of an entire city as well as an area truncated of urban canopy. Such a rendering of urban surface quality may be useful for important tasks such as predicting stages of development bordering natural areas, where intense development may be detrimental to the environment. NDCCI, when composited with NBI and BAEI, can be utilized to classify stages of urban intensity effectively.

The development of urban growth geosimulation models meant to bolster management efforts may become the research frontier for all efforts to mitigate human-driven environmental impacts. Satellite data are generated continuously and serve as an excellent basis for the LULC maps necessary for geosimulations to operate. NBI can be used to extract predictable geometries, BAEI can be reclassified into value ranges describing predictable gradient development, and the NDCCI/NBI/BAEI composite maps can be used to facilitate predictions of fluctuating urban intensity. While it is beyond the scope of this paper to give further consideration to these ideas, the novel method incorporating the BAEI as a shadow index is a clear example of the type of geostatistical

model that can be created to monitor a city's internal growth. Forward, it should also serve as a primary example of the type of success that may be gleaned from geosimulation models based on focal analysis in general.

References

Abbas, A.W., Ahmad, N., Abid, S.A.R., & Khan, M.A.A. (2016). K-means and ISODATA Clustering Algorithms for Landcover Classification Using Remote Sensing. *Sindh University Research Journal (Sci. Ser.) 48*(2), 315-18.

As-syakur, A., Adnyana, I., Arthana, I., & Nuarsa, I. (2012). Enhanced Built-up and Bareness Index (EBBI) for Mapping Built-up and Bare Land in an Urban Area. *Remote Sensing, 4*(10), 2957-970.

Ball, G.H., & Hall, D.J. (1965). *Isodata: A Method of Data Analysis and Pattern Classification.* Menlo Park, CA: Stanford Research Institute.

Beck, L., Hutchinson, R., & Zauderer, C. (1990). A Comparison of Greenness Measures in Two Semi-arid Grasslands. *Climatic Change, 17*(2-3), 287-303.

Benkouider, F., Abdellaoui, A., Hamami, L. (2019). New and Improved Built-up Index Using SPOT Imagery: Application to an Arid Zone (Laghouat and M'Sila, Algeria). *Journal of the Indian Society of Remote Sensing, 47*(2), 185-92.

Bouzekri, S., Lasbet, A., & Lachehab, A. (2015). A New Spectral Index for Extraction of Built-up Area Using Landsat-8 Data. *Journal of the Indian Society of Remote Sensing, 43*(4), 867-73.

Cabral, P. (2007). Délimitation D'aires Urbaines à Partir D'une Image Landsat ETM: Comparaison de Méthodes de Classification. *Canadian Journal of Remote Sensing, 33*(5), 422-30.

Chrysoulakis, N. (2003). Estimation of the All-wave Urban Surface Radiation

Balance by use of ASTER Multispectral Imagery and In Situ Spatial Data. *Journal of Geophysical Research: Atmospheres, 108*(D18).

Clark Labs (2015). *TerrSet Geospatial Monitoring and Modeling Software: Version 18.* Worcester, MA.

Cortes, C. & Vapnik, V. (1995). Support-vector Networks. *Machine Learning, 20,* 273–97.

Environmental Systems Research Institute (ESRI). (2020). *ArcGIS Pro Release 2.5.1.* Redlands, CA.

Ettehadi O.E., Kaya, S., Elif, S., & Alganci, U. (2019). Separating Built-up Areas from Bare Land in Mediterranean Cities Using Sentinel-2A Imagery. *Remote Sensing 11*(3), 345.

Gu, L., Cao, Q., & Ren, R. (2018). Building Extraction Method Based on the Spectral Index for High-resolution Remote Sensing Images Over Urban Areas. *Journal of Applied Remote Sensing, 12*(4), 1.

Guan, D., Li, H., Inohae, T., Su, W., Nagaie, T., & Hokao, K. (2011). Modeling Urban Land Use Change by the Integration of Cellular Automaton and Markov Model. *Ecological Modelling, 222*(20), 3761-772.

Han, G., Xu, J. (2013). Land Surface Phenology and Land Surface Temperature Changes Along an Urban-Rural Gradient in Yangtze River Delta, China. *Environmental Management, 52*(1)*,* 234-49.

He, C., Shi, P., Xie, D., & Zhao, Y. (2010). Improving the Normalized Difference Built-

up Index to Map Urban Built-up Areas Using a Semiautomatic Segmentation Approach. *Remote Sensing Letters, 1*(4), 213-21.

Hochmair, H. Gann, D., Benjamin, A., & Fu, J. (2016) Miami-Dade County Urban Tree Canopy Assessment. *GIS Center*. 65. Retrieved December 15, 2019 from https://digitalcommons.fiu.edu/gis/65/

Igun, E. (2017). Analysis and Sustainable Management of Urban Growth's Impact on Land Surface Temperature in Lagos, Nigeria. *Journal of Remote Sensing & GIS 6*(212).

Jieli, C., Manchun, L., Yongxue, L., Chenglei, S., & Wei, H. (2010). Extract Residential Areas Automatically by New Built-up Index. *2010 18th International Conference on Geoinformatics, 1*(5).

Jin, S., Homer, C., Yang, L., Danielson, P., Dewitz, J., Li, C., Zhu, Z., Xian, G., & Howard, D. (2019). Overall Methodology Design for the United States National Land Cover Database 2016 Products. *Remote Sensing, 11*(24), 2971.

Kim, J., Steiner, R. & Yang, Y. (2014). The Evolution of Transportation Concurrency and Urban Development Pattern in Miami-Dade County, Florida. *Urban Affairs Review, 50,* 672-701.

Marius, P., Balas, V., Perescu-Popescu, L., & Mastorakis, Nikos. (2009). Multilayer Perceptron and Neural Networks. *WSEAS Transactions on Circuits and Systems, 8,* 579-588.

Mohan, M., Kandya, A. (2015). Impact of Urbanization and Land-use/Land-cover

Change on Diurnal Temperature Range: A Case Study of Tropical Urban Airshed of India Using Remote Sensing Data. *Science of the Total Environment, 506-07,* 453-65.

Nelson, K.C., Palmer, M.A., Pizzuto, J.E., Moglen, G.E., Angermeier, P.L., Hilderbrand, R.H., Dettinger, M., Hayhoe, K. (2009). Forecasting the Combined Effects of Urbanization and Climate Change on Stream Ecosystems: From Impacts to Management Options. *Journal of Applied Ecology, 46*(1), 154-63.

Pal, M. & Mather, P. (2005). Support Vector Machines for Classification in Remote Sensing. *International Journal of Remote Sensing, 26,* 1007-011.

Pei, F., Wu, C., Liu, X., Li, X., Yang, K., Zhou, Y., Wang, K., Xu, L., Xia, G. (2018). Monitoring the Vegetation Activity in China Using Vegetation Health Indices. *Agricultural and Forest Meteorology, 248,* 215-27.

Rahimi, A. (2016). A Methodological Approach to Urban Land-use Change Modeling Using Infill Development Pattern—A Case Study in Tabriz, Iran. *Ecological Processes, 5*(1), 1-15.

Rasul, A., Balzter, H., Ibrahim, G.R.F., Hameed, H.M., Wheeler, J., Adamu, B., Ibrahim, S., & Najmaddin, P.M. (2018). Applying Built-up and Bare-Soil Indices from Landsat 8 to Cities in Dry Climates. *Land, 7*(3), 81.

Samsudin, S.H., Shafri, H.Z.M., & Hamedianfar, A. (2016). Development of Spectral Indices for Roofing Material Condition Status Detection Using Field

Spectroscopy and WorldView-3 Data. *Journal of Applied Remote Sensing, 10*(2), 025021.

Seto, K.C., Güneralp, B., Hutyra, L.R. (2012). Global Forecasts of Urban Expansion to 2030 and Direct Impacts on Biodiversity and Carbon Pools. *Proceedings of the National Academy of Sciences of the United States of America. 109*(40), 16083-088.

Sun, H., Forsythe, W., & Waters, N. (2007). Modeling Urban Land Use Change and Urban Sprawl: Calgary, Alberta, Canada. *Networks and Spatial Economics, 7*(4), 353-76.

Tang, H., Li, Z., Zhu, Z., Chen, B., Zhang, B., Xin, X. (2015). Variability and Climate Change Trend in Vegetation Phenology of Recent Decades in the Greater Khingan Mountain Area, Northeastern China. *Remote Sensing, 7*(9), 11914-932.

United Nations Department of Economic and Social Affairs (UN DESA) (2017, June 21). World Population Projected to Reach 9.8 Billion in 2050, and 11.2 Billion in 2100. Retrieved December 15, 2020, from https://www.un.org/development/desa/en/news/population/world-population-prospects-2017.html

United States Geological Survey (USGS). (n.d.). *Landsat Surface Reflectance.* Retrieved April 12, 2020, from https://www.usgs.gov/land-resources/nli/landsat/landsat-surface-reflectance

Waqar, M.M., Mirza, J.F., Mumtaz, R., & Hussain, E. (2012). Development of New Indices for Extraction of Built-up Area & Bare Soil from Landsat Data. *Open Access Scientific Reports, 1*(1).

World Population Review. (2020). *Miami, Florida Population 2020.* Retrieved April 12, 2020, from http://worldpopulationreview.com/us-cities/miami-population/

Xu, H. (2008). A New Index for Delineating Built-up Land Features in Satellite Imagery. *International Journal of Remote Sensing, 29*(14), 4269-276.

Zha, Y., Gao, J., & Ni, S. (2003). Use of Normalized Difference Built-up Index in Automatically Mapping Urban Areas from TM Imagery. *International Journal of Remote Sensing, 24*(3), 583-94.

Zia, S., Shirazi, S.A., Bhalli, M.N., Kausar, S. (2015). The Impact of Urbanization on Mean Annual Temperature of Lahore Metropolitan Area, Pakistan. *Pakistan Journal of Science, 67*(3), 301-07.